Journal of Luminescence 242 (2022) 118571

Contents lists available at ScienceDirect

Journal of Luminescence

journal homepage: www.elsevier.com/locate/jlumin

Spectrographic analysis of zinc-sulfate-magnesium-phosphate glass containing neodymium ions: Impact of silver–gold nanoparticles plasmonic coupling

N.N. Yusof [a], S. Hashim [b,*], S.K. Ghoshal [a], M.N. Azlan [c], M.H.M. Zaid [d], Imed Boukhris [e,f], Imen Kebaili [e,g]

[a] Physics Department, Faculty of Science, Universiti Teknologi Malaysia, 81310, Johor Bahru, Johor, Malaysia
[b] Centre for Sustainable Nanomaterials (CSNano), Ibnu Sina Institute for Scientific and Industrial Research (ISI-SIR), Universiti Teknologi Malaysia, 81310, Skudai, Johor, Malaysia
[c] Physics Department, Faculty of Science and Mathematics, Sultan Idris Education University, 35900, Tanjung Malim, Perak, Malaysia
[d] Physics Department, Faculty of Science, Universiti Putra Malaysia, 43400, UPM, Serdang, Selangor, Malaysia
[e] Department of Physics, Faculty of Science, King Khalid University, P.O. Box 9004, Abha, Saudi Arabia
[f] Université de Sfax, Faculté des Sciences de Sfax, Département de Physique, Laboratoire des Matériaux Composites Céramiques et Polymères (LaMaCoP) Faculté des Sciences de Sfax BP 805, Sfax, 3000, Tunisia
[g] Laboratoire de Physique Appliquée, Groupe des Matériaux Luminescents, Université de Sfax, Faculté des Sciences de Sfax, BP 1171, 3000, Sfax, Tunisia

ARTICLE INFO

Keywords:
Glass
Optical properties
Spectroscopy
Nanoparticles

ABSTRACT

Ascertaining plasmonic interaction induced by silver (Ag) and gold (Au) nanoparticles (NPs) in the amorphous system can open a new direction in photonics. In this outlook, various contents of Ag and Au NPs were incorporated into neodymium ions (Nd^{3+})-doped zinc-sulfate-magnesium-phosphate glasses via the melt-quenching method. The impact of Ag–Au plasmonic coupling on the structures and spectroscopic traits of the prepared glasses were evaluated. As-quenched samples were analyzed using XRD, HRTEM, Raman, absorption and photoluminescence (PL) spectrometer. The Judd-Ofelt (JO) theory was used to evaluate the spectroscopic quality and stimulated emission cross-section of the glasses. HRTEM micrographs verified the existence of Au and Ag NPs in the glass matrix with a mean size ranged 4.47–7.03 nm. The observed thirteen absorption bands centered around 326, 352, 430, 459, 473, 512, 52, 581, 627, 681, 744, 801, and 875 nm were corresponding to electronic transitions from the ground state ($^4I_{9/2}$) to the excited states of $^4D_{7/2}$, $^2D_{1/2}+^4D_{3/2}+^4D_{5/2}$, $^2P_{1/2}$, $^4G_{11/2}$, $^2D_{3/2}+^2P_{3/2}+^2G_{9/2}$, $^4G_{9/2}+^2K_{13/2}$, $^4G_{7/2}$, $^4G_{5/2}+^2G_{7/2}$, $^2H_{11/2}$, $^4F_{9/2}$, $^4F_{7/2}+^4S_{3/2}$, $^4F_{5/2}+^2H_{9/2}$ and $^4F_{3/2}$ in Nd^{3+}. Two surface plasmon resonance (SPR) bands assigned to Ag and Au NPs were probed at 442 nm and 503 nm. The addition of Au NPs causes the SPR band of Ag NPs to be red-shifted. The NIR PL bands at 878 nm, 1050 nm and 1322 nm were due to the $^4F_{3/2} \rightarrow {}^4I_{9/2}$, $^4F_{3/2} \rightarrow {}^4I_{11/2}$ and $^4F_{3/2} \rightarrow {}^4I_{13/2}$ transitions, respectively. The PMZ1.5Nd0.5Ag0·1Au glass disclosed the highest bandwidth gain of 6.92, 17.05 and 9.10 ($\times 10^{-23}$ cm^3) corresponding to the $^4F_{3/2} \rightarrow {}^4I_{9/2}$, $^4F_{3/2} \rightarrow {}^4I_{11/2}$ and $^4F_{3/2} \rightarrow {}^4I_{13/2}$ transitions. It was shown that the PL intensity of the studied glasses could be modified by varying Ag and Au NPs contents. The Ag–Au NPs plasmonic coupling inclusion inside the glass can be beneficial to develop versatile optical materials.

1. Introduction

For the past decade, metal nanoparticles (NPs) such as silver (Ag) and gold (Au) received great attention due to their peculiarities surface plasmon resonance (SPR) properties that are frequently used in biomedical applications as nanosensors [1] and drug carriers [2]. The Ag or Au NPs have been embedded into the rare-earth ion (REI) doped glass matrix to enhance the REI luminescence intensity and the stimulated emission cross-section [3]. These properties require further improvement to elevate the glass reliability as a solid-state laser

; NPs, Nanoparticles; REI, Rare-earth ions; SPR, Surface plasmon resonance; LSPR, Local surface plasmon resonance; Ag, silver; Au, gold; JO, Judd-Ofelt; PL, Photoluminescence; NIR, Near-infrared.

* Corresponding author.
E-mail address: suhairul@utm.my (S. Hashim).

https://doi.org/10.1016/j.jlumin.2021.118571
Received 9 August 2021; Received in revised form 20 September 2021; Accepted 1 November 2021
Available online 10 November 2021

amplifier. The Web of Science database presents 158 articles (1970–September 15, 2021) using the keyword: silver and gold nanoparticles embedded glass. From the 158 documents extracted, only 14 articles discussed the behaviour of Ag and Au NPs situated in disordered materials [4–17]. The plasmon-plasmon interactions in oxoanionic glass such as nitrates, sulfates, carbonates, hydrates−based glass has not been fully understood [18,19]. Prospectively, these glasses would be compelling for solid-state laser applications. It is worth mentioning that the SPR resulted from high charge carrier concentration NPs (10^{22} cm^{-3}) resonant with the incoming electromagnetic wave [20]. Coupling two metal NPs could generate bonding dimer plasmon (BDP) and creates a hot spot junction of the local field that subsequently raised the electron responsible for luminescence action [21]. Previous studies revealed that the amalgamation of Ag (0.9 mol%) and Au NPs (0.15 mol%) with Eu^{3+} doped magnesium-zinc-sulfophosphate glass has raised REIs emission cross-section [17]. Although the nucleation and growth mechanism Ag–Au core-shell structure inside the glass has not been fully explained, the result demonstrates luminescence enhancement via SPR [17]. The glass transparency and refractive index also increased with Ag and Au NPs embedment, making them captivating for many applications such as in laser amplifiers, photonic devices, optical sensors, light-emitting diodes (LED's), photovoltaic and optical data [1]. Nevertheless, research associated with metal NPs co-embedment into the REIs doped glass is rarely published; to cite a few [22–24].

In addition to the attractive properties of Ag and Au NPs, the glass composition (comprises REIs, glass modifier and glass former) are equally important to maximize the efficiency of host glass as an amplifier. Among the REI, neodymium (Nd^{3+}) ion has great NIR lasing transitions at $^4F_{3/2} \rightarrow {}^4I_{11/2}$ located about 1.06 μm that potential for high-power lasers application. Besides, PL around 1.33 μm corresponds to $^4F_{3/2} \rightarrow {}^4I_{13/2}$ already employed for optical amplifiers and telecommunications [25]. Meanwhile phosphorus pentoxide (P_2O_5) as glass former able to dissolve high concentration of REI ($\approx 10^{21}$ ions/cm^3) without agglomeration which is fifty times better than silicate as glass host [26]. Phosphate glass has been used in many active devices with high energy storage capabilities. Particularly, Nd^{3+} based phosphate glass are broadly commercialized as laser glass in the optical industry such as Schott, (LG-750, LG-760 and LG-770), Hoya Corporation (LHG-80, LHG-8 and LHG-5), Kigre (Q88 and Q98) and N21 and N31 laser glass from Shanghai [21,27] Furthermore, the hygroscopic character of phosphate glass could be overcome by insertion of sulfate ions, magnesium and zinc cation into the network [28]. The inclusion of $ZnSO_4$ eases the glass forming process and raised the thermal and chemical stability of the glass [18]. The addition of MgO further improved the chemical resistance of the glass by creating bond/linkers with phosphate ions [29]. Besides, the interaction of sulfate (SO_4^{2-}) and metaphosphate () creates an excellent environment for REI to be distributed within the glass matrix; due generation of dynamic concentrations of the dithiophosphates (DTPs) units [20,30]. Despite the great potential of zinc-sulfate-magnesium phosphate glass system with Nd^{3+} ion doping, the role of Ag and Au NPs as synergistic sensitizers in REI-doped glass has not been further examined.

The demand for glass-based economic laser hosts is ever increasing. Based on this concern, Nd^{3+}−doped zinc-sulfate-magnesium phosphate glass is synthesized using the melt-quenching technique, which is incorporated with a low concentration of metal NPs (both Ag and Au NPs). The physical, structural and optical properties of the glass were securitized. The Judd-Ofelt (JO) intensity and radiative parameters were calculated to establish a correlation between theoretical and experimental data. The JO parameter gather could assist in evaluating the glass capability as a laser host. The results were interpreted and further discussed to provide useful information in developing advanced optical materials.

2. Experimental

2.1. Glass preparation

The glass composition $58.5P_2O_5$–20MgO–$20ZnSO_4$–$1.5Nd_2O_3$–0.5 Ag NPs−Au NPs (where $x = 0.1$, 0.2, 0.3 and 0.4, mol% in excess) were synthesis via melt-quenching technique. The concentration of Ag NPs has remained fixed meanwhile concentration of Au NPs was varied. The glass code is listed in Table 1 meanwhile the image of the glass is displayed in Fig. 1. The contents of Nd_2O_3 (1.5 mol%) and Ag NPs (0.5 mol %) were selected based on optimum PL intensity shown in previous work [3,31]. Another three glasses were prepared to probe the SPR of Ag and Au NPs. The present work used high purity ≈99.9% raw material (powdered form) purchased from Sigma Aldrich. The diameter of metal NPs was verified below 100 nm before being subjected to heat. About 22 g of mixed constituent raw material was placed in an alumina crucible before it been preheated at 300 °C for 30 min. The pre-heating constitutes then heated at 1100 °C for 1.5 h. The preheated process is essential to reduce OH^- content that contributes high phonon energy to the glass. The mixed powdered material that turns to semi-liquid melt later been poured on top of preheated stainless−steel plate that has been annealed at 300 °C for 3 h. The annealing process helps to avoid possible crystallization and mechanical shock or thermal stress from the supercooling process. The glass was let cool to room temperature and collected the next day. It is kept in vacuum desiccators to avoid atmospheric moisture. The glass is cut and polished to a thickness of ±0.3 cm for better optical (absorption and photoluminescence) measurement. These finishing treatments is required to minimize the scattering effect from an uneven surface.

2.2. Glass characterization

The characterization and formulae for a physical parameter are referred from the previous work [32]. X-ray diffraction (XRD) pattern is measure using PANalytical X'Pert PRO MRD PW3040 with Cu Kα radiations (λ = 1.54 Å) in scanning angle of 2θ ranging between 20° and 80°, step width 0.02° with scan speed 4.0628°/min, functioning at 40 kV and 35 mA to approve the amorphous nature of the glass. The HORIBA Scientific Raman LABRam HR Evolution Spectrometer (Helium–Neon laser) was used to evaluate bonding properties from Raman spectra. A high-resolution transmission electron microscope (HRTEM, JEOL 2100 F) work at an acceleration voltage of 200 kV was used to probe metal NPs existence and size. The absorption spectra of the prepared glasses were recorded by A Shimadzu UV-3600 spectrophotometer. The PL emission and decay measurement is attained through The PTI QuantaMaster™ 60 Fluorescence Spectrophotometer using NIR PMT detector, R550 and excites at 802 nm, supported by liquid nitrogen. Using ellipsometer (J.A. Woolan M − 2000 U), the refractive index, n of the glass is measured in the range 400–1000 nm with incidence angle 75° (Brewster's angle) to computed JO analysis. The sample was characterized at room temperature (≈27 °C). Details formulae of Judd-Ofelt

Table 1
Prepared glass composition and code.

Glass composition	Glass Code
$58.5P_2O_5$–20MgO–$20ZnSO_4$–$1.5Nd_2O_3$–0.5 Ag NPs	PMZ1.5Nd0.5 Ag
$58.5P_2O_5$–20MgO–$20ZnSO_4$–$1.5Nd_2O_3$–0.5 Ag NPs−0.1 AuNPs	PMZ1.5Nd0.5Ag0·1Au
$58.5P_2O_5$–20MgO–$20ZnSO_4$–$1.5Nd_2O_3$–0.5AgNPs−0.2Au NPs	PMZ1.5Nd0.5Ag0·2Au
$58.5P_2O_5$–20MgO–$20ZnSO_4$–$1.5Nd_2O_3$–0.5AgNPs−0.3Au NPs	PMZ1.5Nd0.5Ag0·3Au
$58.5P_2O_5$–20MgO–$20ZnSO_4$–$1.5Nd_2O_3$–0.5AgNPs−0.4Au NPs	PMZ1.5Nd0.5Ag0·4Au
$58.5P_2O_5$–20MgO–$20ZnSO_4$—0.5AgNPs	PMZ0.5 Ag
$58.5P_2O_5$–20MgO–$20ZnSO_4$–0.5Au NPs	PMZ0.5Au
$58.5P_2O_5$–20MgO–$20ZnSO_4$–0.5AgNPs−0.5Au NPs	PMZ0.5Ag0·5Au

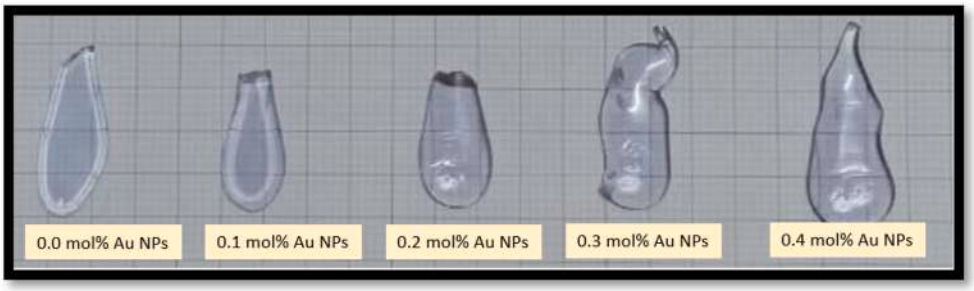

Fig. 1. The photograph of the glass at different Au NPs concentrations (mol%).

theory could be referred in previous published papers; to cite a few [33–35]. Equations (1) and (2) were used to calculate the Racah parameter (*B* and *C*) [36,37].

$$B = \frac{2\nu_3^2 + \nu_2^2 - 3\nu_3\nu_2}{15\nu_2 - 27\nu_3} \tag{1}$$

$$C = \frac{\nu_1 - 4B - 10Dq}{3} \tag{2}$$

where ν_1, ν_2 and ν_3 are first three highest energy absorption transition and Dq is crystal field strength which yields

$$Dq = \frac{\nu_3}{10} \tag{3}$$

The absorption band of Nd^{3+} ions would be slightly influenced by the ligand field interaction associated with electron repulsion within the 4f shell. The crystal field strength (Dq) and Racah parameter (B, C) are typically used to reflect the possible interaction [38]. The bonding formation can be further determined by calculating the nephelauxetic functions of the ligand h_b by following relation [39]:

$$h_b = \frac{(B_{free} - B)/B_{free}}{k_{Nd^{3+}}} \tag{4}$$

where the value of gaseous ion is label as B_{free} ($B_{free} = 331.57$ nm for Nd^{3+} ion) [40]. Meanwhile, the value for the central Nd^{3+} ion $k_{Nd^{3+}}$ is 0.49. Increase of h_b suggesting increases of covalency bond inside the glass matrix where the electron in *f* orbitals delocalize and overlapped with ligand orbitals [36]. The is determine using equation (5)

$$k_{ion} = [(Z + 2 - S)/5]^2 \tag{5}$$

where Z is denoted as the valence of Nd^{3+} ion and S is the spin at the ground state. Herein, Z is 3 and S is 1.5, where 2 S + 1 = 4 [36,38]. Meanwhile, the PL lifetime curve was fitted using a bi-exponential function that express as

$$I(t) = A_1 \exp\left(\frac{-t}{\tau_1}\right) + A_2 \exp\left(\frac{-t}{\tau_2}\right) \tag{6}$$

where I(t) is PL intensity in the function of time, A_1 and A_2 are constant parameters, t is the time, τ_1 and τ_2 are fast and slow lifetime for coefficients A_1 and A_2 respectively. The mean of the measured lifetime was calculated via

$$\tau_{exp} = \frac{A_1\tau_1^2 + A_2\tau_2^2}{A_1\tau_1 + A_2\tau_2} \tag{7}$$

The quantum efficiency follow the formula

$$\eta = \frac{\tau_{exp}}{\tau_{rad}} \times 100 \tag{8}$$

where τ_{exp} and τ_{rad} are experimental and calculated radiative PL lifetime, respectively [41]. The energy transfer (ET) efficiency is estimated by equation

$$E_{ET} = 1 - \frac{\tau_{AgAu}}{\tau_{Ag}} \tag{9}$$

where E_{ET} is the energy transfer efficiency, τ_{AgAu} is PL lifetime containing Au NPs contents (0.1–0.4 mol%) and τ_{Ag} is PL lifetime without Au NPs inclusions [42]. The non-radiative decay rate (W_{NR}) determine through equation [43].

$$W_{NR} = \frac{1}{\tau_{exp}} - \frac{1}{\tau_{rad}} \tag{10}$$

3. Results and discussion

3.1. Physical properties

The physical properties of the prepared glass are enlisted in Table 2. The glass density improved with Au NPs contents up to 0.4 mol% (from 2.70 to 2.74 g cm^{-3}) meanwhile the molar volume shows the reverse trends (from 57.01 to 56.46 cm^{-3}). The Au NPs could allocate themselves within the interstitial spaces in the network and increases the glass compactness [44]. However, Au NPs is inclined to distort the phosphate chains and added more free spaces within the network, especially when added at high concentrations (0.4 mol%) [42,45] This disorder could modify the number of NBO bonds and subsequently alter the stoichiometry and the optical parameters of the glass [45,46]. On

Table 2
Physical properties of the synthesis glasses.

Physical Parameters	0.0 mol % Au	0.1 mol % Au	0.2 mol % Au	0.3 mol % Au	0.4 mol % Au
Density (±0.007 g cm^{-3})	2.70	2.71	2.72	2.74	2.73
Molar volume (±0.007 cm^{-3})	57.01	56.96	56.85	56.46	56.70
Direct band gap (±0.01 eV)	4.095	4.065	4.063	4.022	4.045
Indirect band gap (±0.01 eV)	3.909	3.909	3.908	3.874	3.904
Urbach Energy (±0.01 eV)	0.182	0.204	0.181	0.186	0.181
Refractive index @633 nm (±0.001)	1.515	1.517	1.516	1.516	1.516
Molar reflection (±0.01)	51.44	51.40	51.29	51.00	51.16
Molar polarizability (× 10^{22} ±0.01)	2.01	2.01	2.01	2.00	2.00
Au atom contents (× 10^{20} atom/cm^3)	0.29	0.57	0.86	1.17	1.45
Polaron radius (× 10^{-7})	2.83	2.24	1.96	1.77	1.64
Inter-nuclear distance (× 10^{-7})	3.27	2.59	2.26	2.04	1.90
Field strength (× 10^{14} cm^{-2})	2.75	4.37	5.75	7.04	8.13

top, the decrease of inter-nuclear distance (3.27–1.90 × 10^{-7}) and polaron radius (2.83–1.64 × 10^{-7}) with Au NPs embedment would increase the strength of Nd–O bonds which associated with the glass' absorption and luminescence properties [44]. It is predicted that the field strength between NPs increases with the addition of Au atom [47]. Herein, field strength refers to the attraction of Coulomb's force between NPs [48]. Previous reports show similarity trends where the variation of physical and optical traits is an attestation of structure adjustment from Au NPs inclusion [42].

The value of direct (4.095–4.022 eV) and indirect (3.909–3.874 eV) band gap of present studies fluctuated at different Au NPs contents. This occurrence was probably due to Ag/Au NPs ability to evoke the nonlinear optical properties of glass from the hyperpolarizabilities induced by the SPR effect [1,45,46]. This explains the see-saw pattern in the value of molar reflection (51.44–51.00), molar polarizability (2.01–2.00 × 10^{22}) and refractive index (1.515–1.517) as well. The Urbach energy depicts the degree of disorders and formation of oxygen vacancies [44]. The sample containing 0.1 mol% Au NPs revealed the highest Urbach energy value (0.204 eV) which is expected to have distinct optical attributes ascribed to the creation of non-bridging oxygens (NBOs) and defects [1].

3.2. XRD patterns

Fig. 2 displays the XRD pattern of the selected sample; PMZ1.5Nd0.5 Ag and PMZ1.50.4Ti0·5Ag0.2Au. No crystalline peak corresponding to Ag and Au NPs were evidenced within the glass network. Only broad hump appeared in range 15–25° which confirms the amorphous nature of the glass. Previous work shows a similar broad hump pattern for glass unless it is heat-treated [49,50]. The low contents of plasmonic NPs have hidden the crystalline peak of embedded metal NPs [21]. To detect co-embedment of Ag and Au NPs incorporated into the sample, the HRTEM microscopy were used to map any possible metal NPs distributed inside the glass.

3.3. HRTEM mapping

Fig. 3 depicts the HRTEM micrograph of the glass containing low (0.2 mol%) and high (0.4 mol%) Au NPs respectively, both incorporated with the same amount of Ag NPs (0.5 mol%). The black spots in the HRTEM mapping indicate the presence of spherical shaped metal NPs within the matrix. No alloy nor core-shell structure is observed as

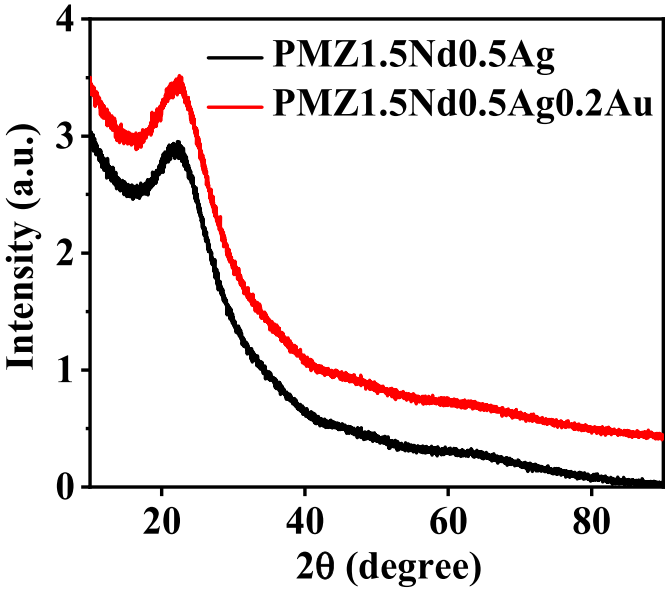

Fig. 2. XRD pattern of PMZ1.5Nd0.5 Ag and PMZ1.5Nd0.5Ag0·2Au.

portrayed in previous work associated with Ag/Au NPs insertion into the glass [17,49,51]. The high melting temperature of the phosphate glass could restrain the nucleation of Ag–Au core-shell nanostructures inside the glass [49]. The presence of Ag and Au NPs is recognized based on ICDD PDF card number Ag (04–0783) and Au (04–0784). The size of metal NPs is measured in the same direction and angle [52]. The statistic distribution function such as Log-normal, Weibull and Gamma were used to estimate the mean size of NPs since it is non-symmetrical distribution. The mentioned functions were claimed to be most appropriate for the continuous and asymmetrical distribution system [32]. The lattice spacing of 0.23 nm (Fig. 4 (a)) and 0.28 nm (Fig. 4 (b)) both matched with lattice planer orientations (111) that belonged to Ag and Au NPs, respectively. The lattice profile for both metal NPs has been depicted in Fig. 5. The mean size of metal NPs for sample PMZ1.5Nd0.5Ag0·2Au is 4.47 nm (Fig. 6 (a)) meanwhile for sample PMZ1.5Nd0.5Ag0·4Au, the value is 7.03 nm (Fig. 6 (b)). In the present glass, the distribution of metal NPs size represent both type of metals NPs (Ag and Au) since the overall size and shape for the metal NPs is relatively similar. The increase of Au NPs concentration leads to enlargement of NPs size [12]. The raising of concentration causes a decrease in the mean spacing between the molecules during the melting process. This urges the metal NPs to get close to each other due to great surface tension between them. The rise of surface tension connecting NPs is attributed to high attractive van der Waals force over the electrostatic repulsion force between the NPs. The improved surface tension facilities NPs growth and subsequently increases NPs sizes [53]. The growth mechanism is commonly referred to as Ostwald ripening process followed by coalescence that increases the NPs size [54]. The crystallization of metal NPs inside the glass could be express by redox reactions. During the melting, Ag^{+} and Au^{3+} ions possibly formed and reduce to neutral Ag and Au NPs during the annealing process. The Ag NPs is formed through $Ag^{+}+e^{-}\rightarrow Ag^{0}$ and Au NPs via $Au^{3+}+3e^{-}\rightarrow Au^{0}$ [24]. Gibb's free energy relation could predict the permissibility of the reaction; either it is spontaneous (possible) or non-spontaneous (hardly possible). When the ΔE^{0} disclosed positive value, ΔG present a negative value which indicates the reaction is possible [3]. Gibb's free energy relation could be express as

$$\Delta G = - kF\Delta E^{0}$$

Here ΔG is the free energy change, k is the molar number, and F is Faraday constant. The redox reaction that could be anticipated inside the glass are listed

$$2P^{3+} + 3Au^{3+} \rightarrow 2P^{5+} + 3Au^{0} \left(\Delta E^{0} = 5.7658\right)$$

$$P^{3+} + 2Ag^{+} \rightarrow P^{5+} + 2Ag^{0} \left(\Delta E^{0} = 2.2351\right)$$

$$P^{3+} + 2Nd^{3+} \rightarrow P^{5+} + 2Nd^{2+} \left(\Delta E^{0} = -4.7641\right)$$

$$P^{3+} + Nd^{2+} \rightarrow P^{5+} + Nd^{0} \left(\Delta E^{0} = -1.6871\right)$$

Based standard redox relation listed, the nucleation of neutral Ag and Au NPs is possible. Meanwhile, Nd^{0} crystallization only occurs in non-spontaneous reactions. The standard reduction potentials () used to estimate the possible reaction is listed

$$Ag^{+}/Ag^{0} = 0.7996 \text{ V}$$

$$Au^{3+}/Au^{0} = 1.498 \text{ V}$$

$$Nd^{3+}/Nd^{2+} = -2.700 \text{ V}$$

$$Nd^{3+}/Nd^{0} = -2.323 \text{ V}$$

$$P^{3+}/P^{5+} = 0.6359 \text{ V}$$

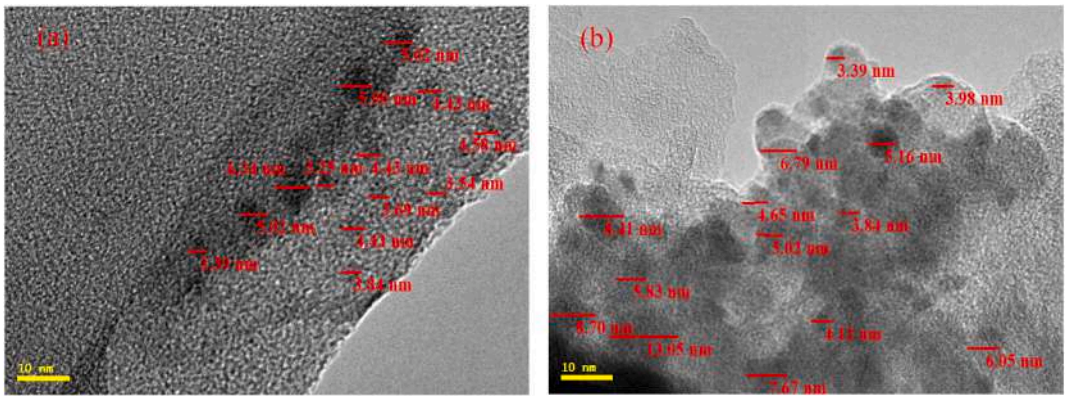

Fig. 3. TEM image of **(a)** PMZ1.5Nd0.5Ag0·2Au and **(b)** PMZ1.5Nd0.5Ag0·4Au.

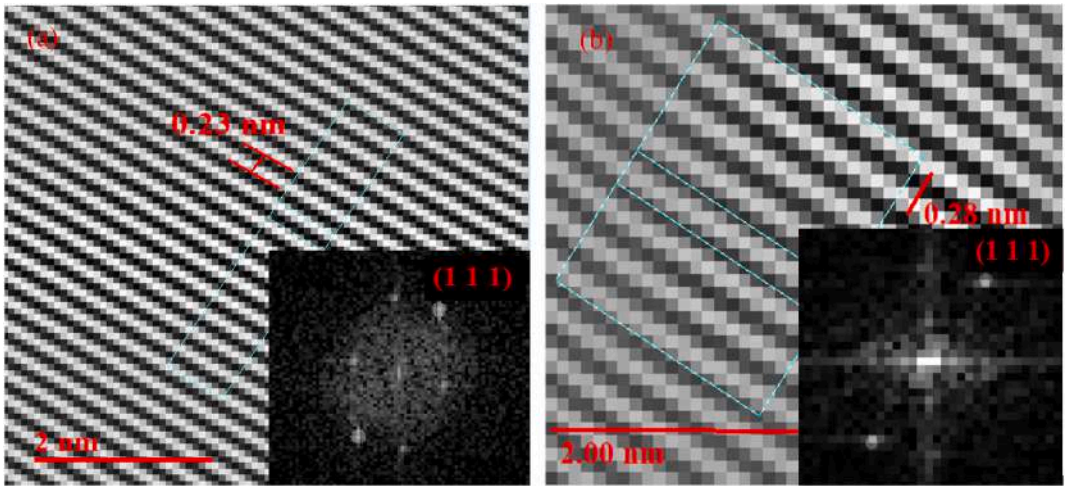

Fig. 4. (a)The lattice spacing of **(a)** Ag NPs and **(b)** Au NPs (insert is FFT of respective NPs).

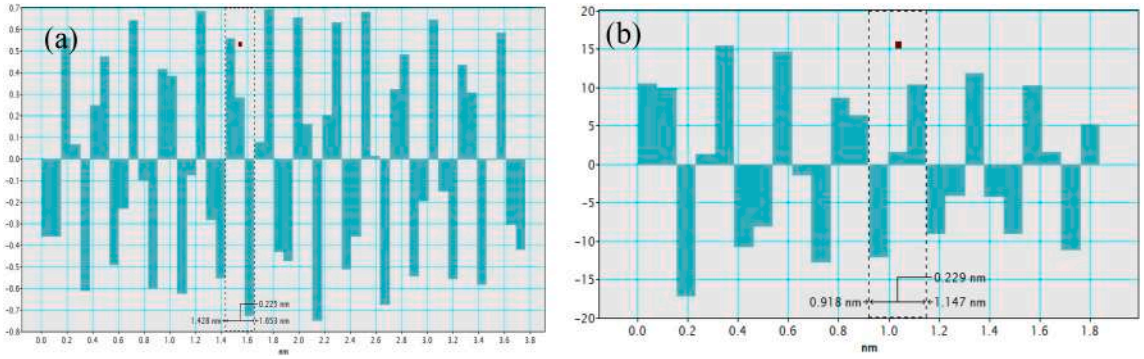

Fig. 5. The lattice profile of **(a)** Ag NPs and **(b)** Au NPs inside the glass sample.

3.4. Raman Spectra

The Raman spectra of selected prepared glass containing different Ag and Au NPs content is depicting in Fig. 7. The Raman spectra show no observable shift for all glass with different Au NPs concentrations. The alteration of Raman intensity could be associated with changes in the local field that affect the overall glass polarizability [30]. The assigned vibration bond is listed:

i. The band located about 337 cm^{-1} is assigned to the bending vibration of P–O–Zn [55,56].
ii. The band positioned about 687 cm^{-1} was approved to P–O–P symmetric stretching of bridging oxygen in Q^2 units [57,58].
iii. The band located at 770 cm^{-1} corresponds to the asymmetric stretching vibration of P–O–P bonds in metaphosphates chains [58,59].
iv. The band appeared at 1202 cm^{-1} allotted to the asymmetric stretching vibration of SO_4^{2-} groups [56,58].
v. The band centered around 1205 cm^{-1} was endorsed to symmetric stretching of $(PO_2)^-$ vibration [54,60].
vi. The band around 1270 cm^{-1} belongs to the asymmetric stretching of non−bridging oxygen $(PO_2)^-$ chains [54,61].

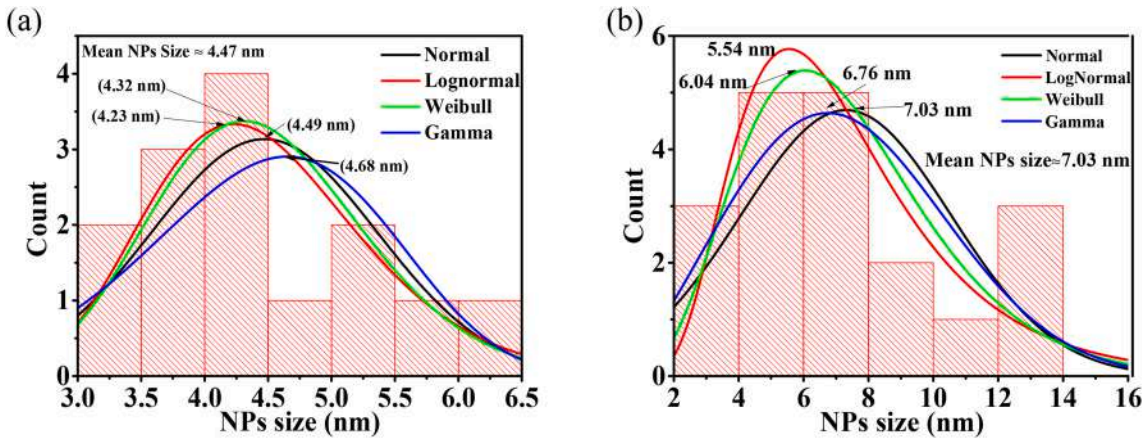

Fig. 6. The metal NPs size distribution in glass **(a)** PMZ1.5Nd0.5Ag0·2Au and **(b)** PMZ1.5Nd0.5Ag0·4Au.

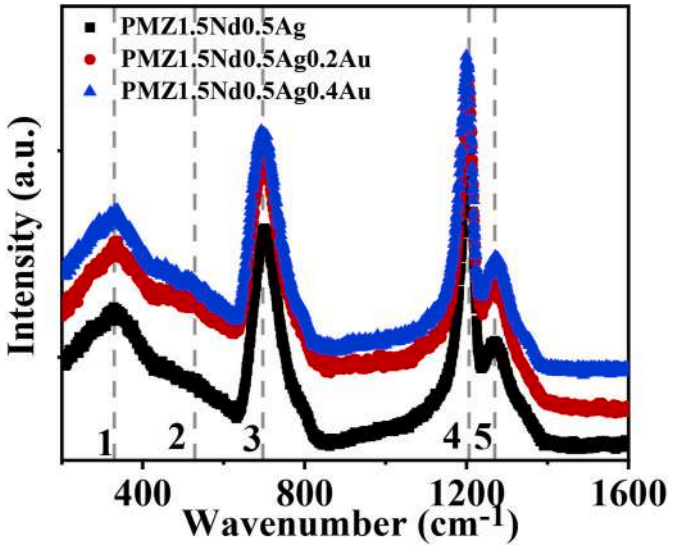

Fig. 7. Raman Spectra of the sample without Au NPs and sample embedded with 0.2 and 0.4 mol% of Au NPs.

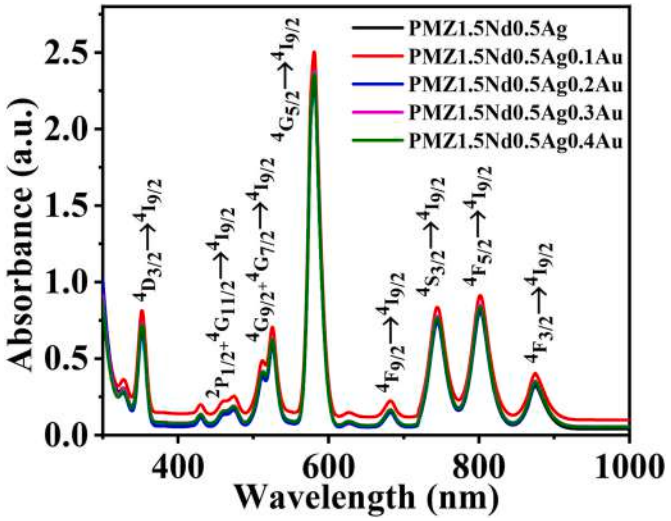

Fig. 8. Absorption spectra of the prepared sample with different Ag–Au NPs contents.

3.5. Absorption spectra

Fig. 8 shows the absorption spectra of glass with different Ag–Au NPs concentrations. Overall, thirteen absorption bands were observed at $^4I_{9/2} \rightarrow {}^4D_{7/2}$ (326 nm), $^4I_{9/2} \rightarrow {}^2D_{1/2}+{}^4D_{3/2}+{}^4D_{5/2}$ (352 nm), $^4I_{9/2} \rightarrow {}^2P_{1/2}$ (430 nm), $^4I_{9/2} \rightarrow {}^4G_{11/2}$ (459 nm), $^4I_{9/2} \rightarrow {}^2D_{3/2}+{}^2P_{3/2}+{}^2G_{9/2}$ (473 nm), $^4I_{9/2} \rightarrow {}^4G_{9/2}+{}^2K_{13/2}$ (512 nm), $^4I_{9/2} \rightarrow {}^4G_{7/2}$ (525 nm), $^4I_{9/2} \rightarrow {}^4G_{5/2}+{}^2G_{7/2}$ (581 nm), $^4I_{9/2} \rightarrow {}^2H_{11/2}$ (627 nm), $^4I_{9/2} \rightarrow {}^4F_{9/2}$ (681 nm), $^4I_{9/2} \rightarrow {}^4F_{7/2}+{}^4S_{3/2}$ (744 nm), $^4I_{9/2} \rightarrow {}^4F_{5/2}+{}^2H_{9/2}$ (801 nm) and $^4I_{9/2} \rightarrow {}^4F_{3/2}$ (875 nm) respectively. The absorption spectra are in agreement with previous studies [3,25,31,62]. The glass incorporated 0.1 mol% of Au NPs show an increment of absorbance. The shielding effect of 4*f* Nd^{3+} ion cause no significant shift observed in all samples [63]. The absorption bands of the glass were compared with aquo−ion values. The nephelauxetic ratios ($\beta = \bar{\nu}_c/\bar{\nu}_a$) and bonding parameters ($\delta = (1-\bar{\beta})/\bar{\beta}$) of samples are enlisted in Table 3. Any shift of absorption spectra is attributed to electron cloud that delocalised within the ligand molecular orbitals which is known as the nephelauxetic effect [21]. Typically nephelauxetic effect (electron cloud expansion) is induced by two ways 1) the effective positive charge of the Nd^{3+} was reduced by the negative charge from the ligands 2) increase of orbital size from the covalent bonding of metal complex (anion-cations) [64]. In present work, sample PMZ1.5Nd0.5Ag0·1Au show ionic character and other sample revealed covalent nature of the glass based on δ values. The electric dipole transition that is more responsive to any ligands or local environment is known as a hypersensitive transition (HST). The HST transition $^4I_{9/2} \rightarrow {}^4G_{5/2}+{}^2G_{7/2}$ followed the selection rule of $|\Delta L| \leq 2$, $|\Delta J| \leq 2$, and $|\Delta S| \leq 0$ and typically show higher absorbance compared to other transitions. Other than JO parameter and nephelauxetic ratios, the Racah parameter is calculated to attain better insight into the spectroscopic behaviour of RE ions and ligand.

3.6. Racah and crystal field strength parameter

The ligand field parameter describes the electrostatic interaction between metal cation (Nd^{3+}) and its ligands (anions: O^{2-} and SO_4^{2-}). Herein, it is worth mentioning that the characteristic of REIs−O bond depending on 1) the local symmetry of Nd^{3+} ion or ligands that surrounded them and 2) the distribution of charge within the 4*f* orbitals (which will affect the bond strength of metal complex). Particularly, Racah parameters *B* and *C* mirrored the magnitude of inter-electronic repulsion from the Nd–O bond, where the distortion in 4*f* orbitals would shift the absorption transition energy of Nd^{3+} ion [66]. Meanwhile, the crystal field strength describes the strength of the bonds. Fig. 9 depicts the absorption bands used to evaluate ligand field parameters (Racah and crystal field strength parameter). It comprised of three prominent absorption band which situated at high energy region

Table 3
Absorption band positions (cm^{-1}), values of aquo, β and δ for prepared glass.

Energy levels	PMZ1.5Nd0.5 Ag	PMZ1.5Nd0.5Ag0·1Au	PMZ1.5Nd0.5Ag0·2Au	PMZ1.5Nd0.5Ag0·3Au	PMZ1.5Nd0.5Ag0·4Au	Aquo [65]
$^4D_{7/2}$	30618.49	30422.88	30599.76	30553.01	30562.35	30,554
$^2D_{1/2}+^4D_{3/2}+^4D_{5/2}$	28409.09	29568.30	28409.09	28409.09	28417.16	28,550
$^2P_{1/2}$	23277.47	25188.92	23282.89	23272.05	23282.89	23,250
$^4G_{11/2}$	21791.24	22624.43	21819.77	21758.05	21781.75	21,650
$^2D_{3/2}+^2P_{3/2}+^2G_{9/2}$	21128.25	21857.92	21114.86	21123.79	21101.5	21,300
$^4G_{9/2}+^2K_{13/2}$	19538.88	20462.45	19527.44	19535.07	19535.07	19,550
$^4G_{7/2}$	19033.12	19368.58	19033.12	19040.37	19036.74	19,160
$^4G_{5/2}+^2G_{7/2}$	17208.74	18089.73	17205.78	17211.7	17214.67	17,380
$^4H_{11/2}$	15959.14	16305.23	15979.55	15966.79	15976.99	15,870
$^4F_{9/2}$	14675.67	15372.79	14667.06	14675.67	14662.76	14,700
$^4F_{7/2}+^4S_{3/2}$	13435.44	14196.48	13437.25	13439.05	13435.44	13,500
$^4F_{5/2}+^2H_{9/2}$	12481.28	12951.69	12479.72	12482.84	12479.72	12,535
$^4F_{3/2}$	11431.18	11859.58	11429.88	11428.57	11431.18	11,460
$\overline{\beta}$	0.997503	1.036712	0.997869	0.997618	0.997661	1
δ	0.002503	−0.03541	0.002135	0.002388	0.002344	0

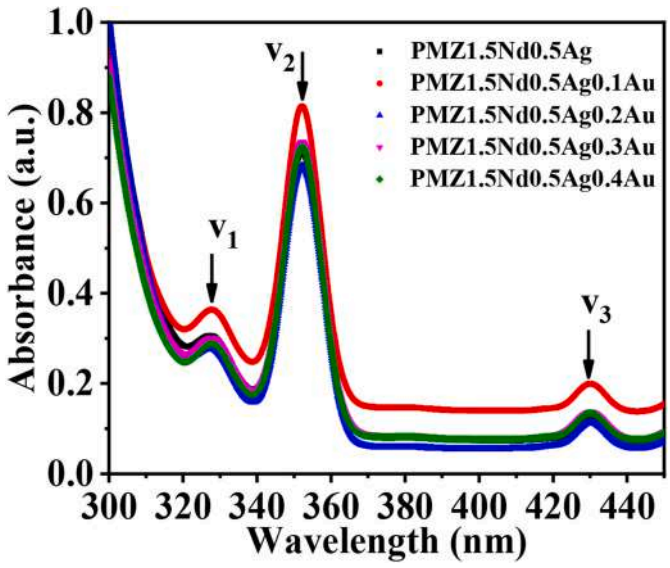

Fig. 9. Three selected absorption bands for Racah and ligand field parameter.

and was assigned as v_1, v_2 *and* v_3 [36]. Table 4 enlists the calculated values of the Racah parameters (*B and C*), crystal field parameters (*Dq, Dq/B*) and Nephelauxetic function (h_b). Initially, the incorporation of Au NPs into the glass reduces the parameter *B* but eventually increase in value after being embedded with 0.3 mol% of Au NPs. Meanwhile, the value of parameter *C* declines as the glass is incorporated with 0.1 mol% of AuNPs and increase slightly when embedded with 0.2–0.4 mol% of Au NPs. The results show that Au NPs able to induces a covalent−ionic nature around Nd^{3+} sites inside the glass. The sample PMZ1.5Nd0.5Ag0·1Au displays the highest h_b (2.015) which indicates the covalent nature of Nd^{3+} ion−ligands improved. The results contradict with bonding parameter, δ data. This occurrence is ascribed to the mixed-modifier effect (MME) which deviated the physical properties from linearity trends due to multiple modifier cations present within the glass [18]. In this case, ionic interactions involving cations and small oxoanions within the glass determine the dynamic of the bonds (i.e covalent or ionic nature) [18]. The sample with 0.1 mol% of Au NPs also shows the highest *Dq* (2518.89) and *Dq/B* (6.54) which indicates its strongest crystal field among the series. Besides, the crystal field strength » 2.3 means the Nd^{3+} ion is confined in a strong crystal field domain [42]. Fig. 10 shows the illustration of the Nephelauxetic effect in response to the Racah parameter. The 4*f* orbital of Nd^{3+} ion expands when the inter-electron repulsion is minimized as the ligands and central metal is covalently bonded [42].

3.7. Surface plasmon resonance (SPR) absorption bands

Three samples (devoid of Nd^{3+} ions) were prepared to detect the SPR absorption bands of Ag, Au and Ag + Au NPs. The SPR band of pure Ag NPs was positioned around 442 nm which is near the absorption edge as elucidated in Fig. 11 (a). Similar to the previous report, the SPR band of Ag NPs inside phosphate glass was located around 442 nm [67]. It was expected that almost perfect spherical Ag NPs will depict a single SPR band around 400–480 nm. Enlargement of the spherical radius (same width and height) would not drastically shift the SPR band unless the dimension of the NPs changed, (e.g rod, star, triangle) [68]. Meanwhile, Au NPs exhibited SPR bands around 509 nm as depicts in Fig. 11(b). The previous report revealed that the SPR band of Au NPs in potassium-aluminium-phosphate glass is located around 520–530 nm, which value is relatively close to the present glass system (509 nm) [69, 70]. The glass containing both Ag and Au NPs show the SPR bands around 463 nm and 503 nm attributed to Ag and Au NPs respectively (Fig. 11(c)). There is no abrupt absorption shift when the glass is embedded with two different types of metal NPs. However, the SPR band appeared to shift toward one another. To explain the possible mechanism of plasmon coupling inside the glass, four paths in the function of the inter-particles distance between Ag and Au NPs is illustrated (Fig. 12) [71]. In the first path, a large interparticle distance between Ag and Au NPs permit them to oscillates according to their natural frequencies [72]. In the second path, when the Ag and Au NPs is substantial close to each other, the SPR band would deviate from their classical

Table 4
The Racah parameters (*B* and *C*), crystal field parameters (*Dq,Dq/B*) and Nephelauxetic function (h_b) values of the prepared glass.

Glass code	*B* (cm^{-1})	*C* (cm^{-1})	*Dq* (cm^{-1})	*Dq/B*	h_b
PMZ1.5Nd0.5 Ag	460.1688	1833.448	2327.747	5.058464	2.009678
PMZ1.5Nd0.5Ag0·1Au	385.2155	1231.033	2518.892	6.538916	2.01475
PMZ1.5Nd0.5Ag0·2Au	459.6249	1826.123	2328.289	5.065628	2.009715
PMZ1.5Nd0.5Ag0·3Au	460.7128	1812.703	2327.205	5.051314	2.009641
PMZ1.5Nd0.5Ag0·4Au	460.4191	1812.594	2328.289	5.05689	2.009661

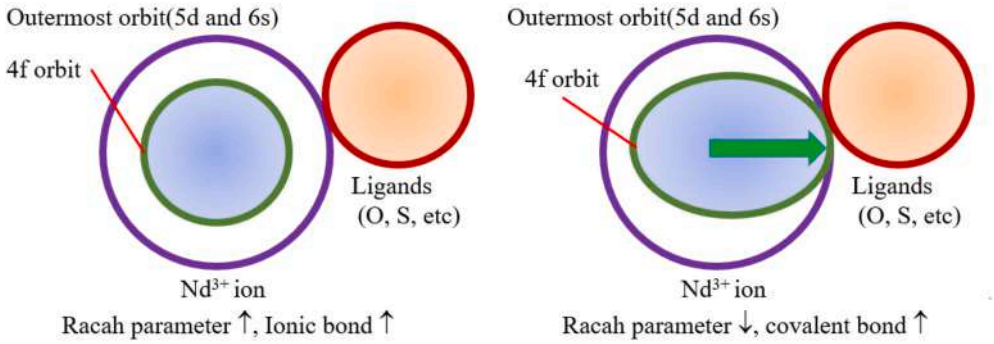

Fig. 10. Illustration of nephelauxetic effect at a different magnitude of Racah parameter.

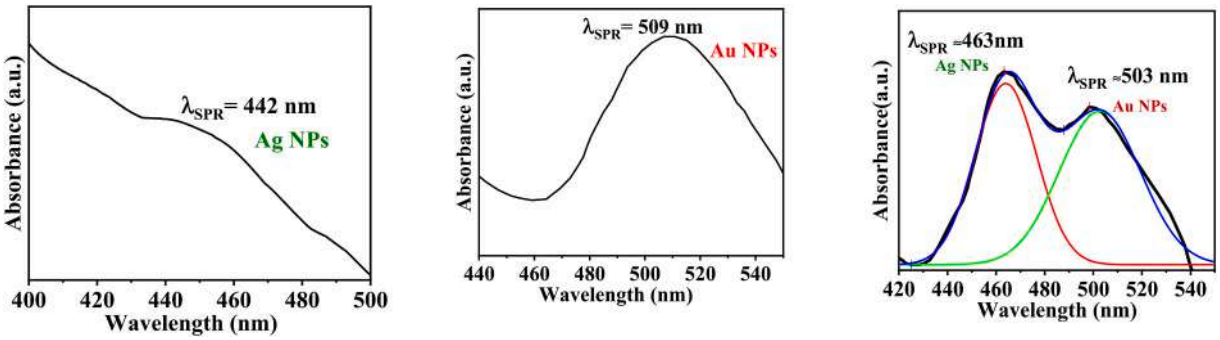

Fig. 11. SPR absorption bands of **(a)** Ag NPs **(b)** Au NPs **(c)** Ag and Au NPs inside the glass.

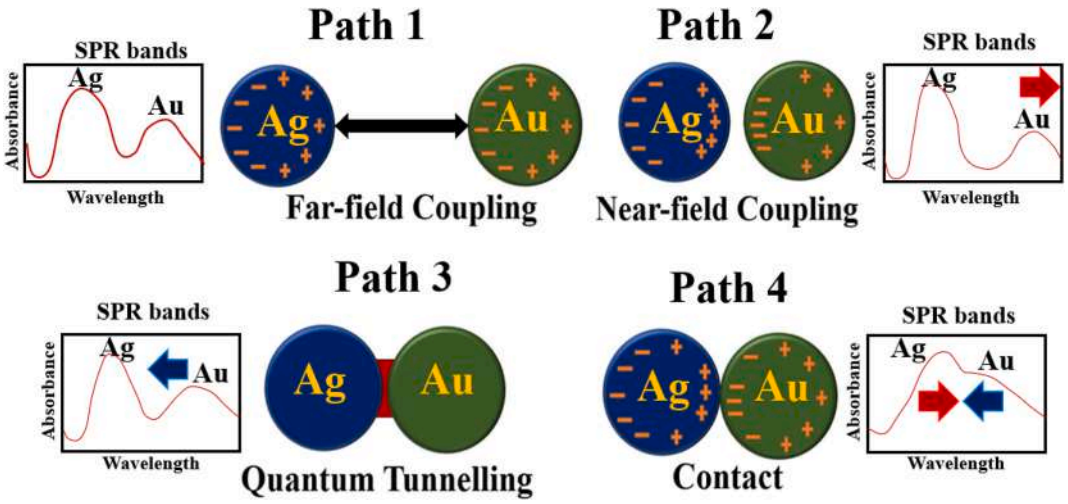

Fig. 12. Illustration of the plasmonic mode at the different spacing of NPs [71].

frequency in response to an external perturbation; a red-shift of the SPR band would be possible. In the third path, the quantum tunnelling effect may be feasible when the distance between NPs is below 1 nm. This shall elevate the hidden quantum effect and made the SPR band appeared to be blue-shift [73]. However in the fourth path, when the interparticle distance of NPs is below 1 nm, the local electromagnetic field would be superimposed and create a new hybrid SPR band [74]. Currently, the SPR band observed is slightly shifted from their original plasmon frequency, yet still consider to oscillated according to their neutral mode (Ag^0 and Au^0) [75]. No SPR band is ascribed to metal−alloy or core-shell NPS inside the glass.

The differences of refractive index in tellurite, germanate and silicate glass containing Ag or Au NPs revealed a slight change in SPR position compare to present glass. The refractive index with a high value would move the SPR band towards a longer wavelength [76–78]. Briefly, the plasmon interaction in Ag–Au NPs depends on their interparticle distance and the dielectric constant of the host glass. A comparative SPR band in a different refractive host is tabulated in Table 5. The Mie scattering theory used to address the relationship of NPs size and dielectric constant, which is expressed as

$$C_{ext} = \frac{24\pi^2 R^3 \varepsilon_m^{3/2}}{\lambda} \cdot \frac{\varepsilon_2}{(\varepsilon_1 + 2\varepsilon_m)^2 + \varepsilon_2^2} \quad (11)$$

the extinction cross-section of the NPS is denoted as C_{ext}, ε_m is the dielectric constant of the glass, λ is radiated wavelength, R is the radius

Table 5
Comparison of refractive index, metal NPs size and their SPR band in varies glass system.

Host glass	Refractive index, n	NPs size (nm)	SPR band (nm)	Refs.
Ag NPs embedment				
$59.0P_2O_5$–20.0MgO–20.0$ZnSO_4$–0.5Sm_2O_3	≈1.78	≈12.50	≈446	[67]
$59.5P_2O_5$–20.0MgO-20.0$ZnSO_4$-0.5Dy_2O_3	≈1.87	≈4.50	≈446	[83]
88.5$NaPO_3$–10ZnO–1Eu_2O_3	≈1.88	≈10.0	≈397	[84]
41.25P_2O_5–41.25Na_2O–15ZnO–0.5Er_2O_3	≈1.43	≈39.0	≈403	[85]
49.0TeO_2–30ZnO–10YF_3–10NaF	≈1.91	≈15.0	≈492	[86]
Au NPs embedment				
6.66B_2O_3–(53.33-*x*)PbO–16GeO_2–4Bi_2O_3–*x*Pr_2O_3,	≈1.97	≈2.8	≈594	[87]
68B_2O_3–15$BaSO_4$–15TeO_2–1Sm_2O_3–1Dy_2O_3	≈1.78	≈29	≈670, 718	[42]
xEr_2O_3–0.8SnO_2–8.3BaO–17.7K_2O–10.0 Al_2O_3–4.7 SiO_2–7.1B_2O_3–(51.3-*x*) P_2O_5	N/A	≈4.0	≈530	[69]
5Sb_2O_3–25Na_2O–69.5B_2O_3–0.5Eu_2O_3	≈1.64	≈8.26	≈581	[45]
50.22 P_2O_5–17.93 K_2O–8.54 BaO–8.45 Al_2O_3–4.80 B_2O_3–2.38 SiO_2–1.02 SnO_2–1.0 Eu_2O_3	N/A	≈7.0	≈524	[70]
Ag and Au embedment				
63.5P_2O_5–20MgO –15$ZnSO_4$–1.5Eu_2O_3	≈1.50	≈27.65	≈463 (Ag), 510 (Au)	[17]
58.5P_2O_5–20.0MgO–20.0$ZnSO_4$–1.5Nd_2O_3	≈1.54	≈7.03	≈463 (Ag), 503 (Au)	Present

of the NPs, ε_1 and ε_2 is real and imaginary part of NPs' dielectric complex, respectively. The SPR is allowed when the condition $\varepsilon_1 = -2\varepsilon_m$ is fulfilled [79,80]. Derived from Mie' scattering theory, the average size of NPs, inside the glass may be estimated via relation [81].

$$R_{NPs} = \frac{\nu_f}{\Delta\omega} \tag{12}$$

where ν_F is the electron velocity at the Fermi surface and $\Delta\omega$ is the full-width half maxima (FWHM) of the SPR absorption bands. The value $\Delta\omega$ can be determined by using the relation $\Delta\omega = 2\pi c \times (1/\lambda_1 - 1/\lambda_2)$ where the speed of light in a vacuum is labelled *c*. The FWHM is calculated and assume the absorption band to be in Gaussian. Meanwhile λ_1 and λ_2 are the wavelengths at FWHM. The value of ν_F for Ag $\approx 1.39 \times 10^{15}$ nms^{-1} [82] meanwhile for gold$\approx 1.40 \times 10^{15}$ nms^{-1} [70]. The average NPs size inside the glass was 4.87 nm and 6.41 nm corresponding to Ag and Au NPs respectively. The addition of Au NPs into the glass could increase the average NPs size.

3.8. Judd ofelt (JO) calculation

The experimental, f_{exp} and calculated, f_{cal} oscillator strength along with root mean square deviation δ_{rms} of prepared glass at different amounts of Au NPs is tabulated in Table 6. The symmetrical Nd^{3+} ions inside the glass system are correlated with oscillator strength. The decrease of oscillator strength indicates high symmetry of structure around Nd^{3+} ion which revealed more ionic nature of the Nd^{3+}–O bonds [88]. The small δ_{rms} values (0.73–1.19 $\times 10^{20}$ cm^2) indicates good oscillator strength fitting. The results show smaller δ_{rms} values compared to other phosphate glass systems [89,90].

Table 7 enlist the JO intensity parameters (Ω_2 Ω_4 Ω_6) and spectroscopic quality $\chi = \Omega_4/\Omega_6$ of the glass. Parameter reflects the nature of Nd^{3+}–O surroundings either low or high polarizability. The rigidity and viscosity of the glass commonly express by Ω_4 and Ω_6 JO parameter [90]. The parameter $\chi = \Omega_4/\Omega_6$ is a preliminary value to predict their laser capability [91]. A decrease of Ω_2 parameter with high Au NPs inclusion (>0.2 mol%) into the glass indicates a high symmetric ligand which is an attestation to the ionic character of Nd^{3+} ions–ligands bond [90]. The lowest value χ disclosed the weakest laser strength as portrayed by glass PMZ1.5Nd0.5Ag0.2Au. Nevertheless, the current glass achieved high χ values compared to some glass systems, as reported from previous work (Table 7). The results demonstrate the role of Au NPs together with Ag NPs in modifying the crystal field symmetry at Nd^{3+} ion site. The high Au NPs contents incorporated into the glass would increase the ionic behaviour of the glass environment. The transition ($^4I_{9/2} \rightarrow {}^4G_{5/2} + {}^2G_{7/2}$) is label as hypersensitive transition and expected to be highly distorted with Au NPs inclusion [92]. The influence of Ag and Au NPs within the glass is further examined through PL analysis.

3.9. NIR PL spectra

Fig. 13 depicts the NIR PL spectra of the selected sample, excited at 802 nm. The spectrum exhibit three prominent NIR PL bands around 878 nm, 1054 nm and 1322 nm which corresponding to $^4F_{3/2} \rightarrow {}^4I_{9/2}$, $^4F_{3/2} \rightarrow {}^4I_{11/2}$ and $^4F_{3/2} \rightarrow {}^4I_{13/2}$ transitions respectively. The PL spectra show typical trends with previous studies, where the highest emission band was observed around 1054 nm [34]. The PL enhancement factor for each glass is tabulated in Table 9. It was determined by divided the

Table 6
Experimental, f_{exp}, calculated, f_{cal} oscillator strength and root mean square deviation δ_{rms} for all glasses.

Transitions from $^4I_{9/2} \rightarrow$	PMZ1.5Nd0.5 Ag		PMZ1.5Nd0.5Ag0·1Au		PMZ1.5Nd0.5Ag0·2Au		PMZ1.5Nd0.5Ag0·3Au		PMZ1.5Nd0.5Ag0.4	
	f_{exp}	f_{cal}	f_{exp}	f_{cal}	f_{exp}	f_{cal}	f_{exp}	f_{cal}	f_{exp}	f_{cal}
$^4D_{7/2}$	2.4539	0.0966	2.5158	0.1008	2.0026	0.0902	2.2574	0.0969	2.2005	0.0958
$^2D_{1/2}+{}^4D_{3/2}+{}^4D_{5/2}$	6.3133	6.0331	6.7031	6.0843	5.093	5.0245	5.8615	5.7139	5.828	5.6723
$^2P_{1/2}$	0.9186	0.4111	1.1569	0.4132	0.3959	0.3383	0.7984	0.3871	0.7439	0.3845
$^4G_{11/2}$	0.4346	0.1145	0.533	0.1188	0.2215	0.105	0.4056	0.1138	0.3818	0.1126
$^2D_{3/2}+{}^2P_{3/2}+{}^2G_{9/2}$	1.2817	0.5034	1.4418	0.5135	0.9981	0.4368	1.1974	0.4859	1.1998	0.4818
$^4G_{9/2}+{}^2K_{13/2}$	1.9887	1.2773	2.1592	1.3244	1.6874	1.1769	1.9227	1.2652	1.9062	1.2531
$^4G_{7/2}$	3.4011	2.6205	3.7259	2.6948	3.1827	2.3733	3.4404	2.5523	3.4198	2.5352
$^4G_{5/2}+{}^2G_{7/2}$	15.4341	15.4832	16.152	16.2176	15.3015	15.3517	15.3436	15.399	15.2995	15.3545
$^4H_{11/2}$	0.2939	0.1019	0.3865	0.1072	0.1312	0.0978	0.2355	0.1037	0.2379	0.1024
$^4F_{9/2}$	0.7024	0.3982	0.8396	0.4201	0.5117	0.3856	0.6343	0.4067	0.6528	0.4015
$^4F_{7/2}+{}^4S_{3/2}$	5.2855	5.0638	5.588	5.3953	5.1136	5.0513	5.396	5.2596	5.3326	5.185
$^4F_{5/2}+{}^2H_{9/2}$	5.8969	6.3677	6.2323	6.6435	5.7193	5.9512	6.0255	6.385	5.9365	6.3119
$^4F_{3/2}$	1.9247	2.9475	0.9207	2.9878	1.8864	2.4989	1.9766	2.8162	1.9614	2.7937
δ_{rms}	0.9574		1.1958		0.7323		0.8716		0.8556	

Table 7
JO intensity parameter Ω_2 Ω_4, Ω_6 and spectroscopic quality $\chi = \Omega_4/\Omega_6$ of prepared glass.

Glass	Ω_2	Ω_4	Ω_6		Ref.
PMZ1.5Nd0.5 Ag	8.59	11.20	6.90	1.62	Present
PMZ1.5Nd0.5Ag0·1Au	9.28	11.26	7.39	1.52	Present
PMZ1.5Nd0.5Ag0·2Au	9.66	9.22	7.01	1.31	Present
PMZ1.5Nd0.5Ag0·3Au	8.88	10.55	7.24	1.46	Present
PMZ1.5Nd0.5Ag0·4Au	8.89	10.48	7.12	1.47	Present
P_2O_5–Al_2O_3–Nd_2O_3	9.06	3.08	1.97	1.56	[93]
TeO_2–ZnO–Na_2O–Nd_2O_3	2.99	2.82	2.62	1.07	[94]
H_3BO_3–Bi_2O_3–$BaCO_3$–CaF_2–7.5ZnO–Nd_2O_3	2.41	0.95	1.15	0.85	[95]
TeO_2–Bi_2O_3–BaO–Nd_2O_3	1.98	0.88	1.83	0.48	[96]
ZnO–Li_2O–Na_2O–P_2O_5–Nd_2O_3	1.93	0.14	3.72	0.03	[34]

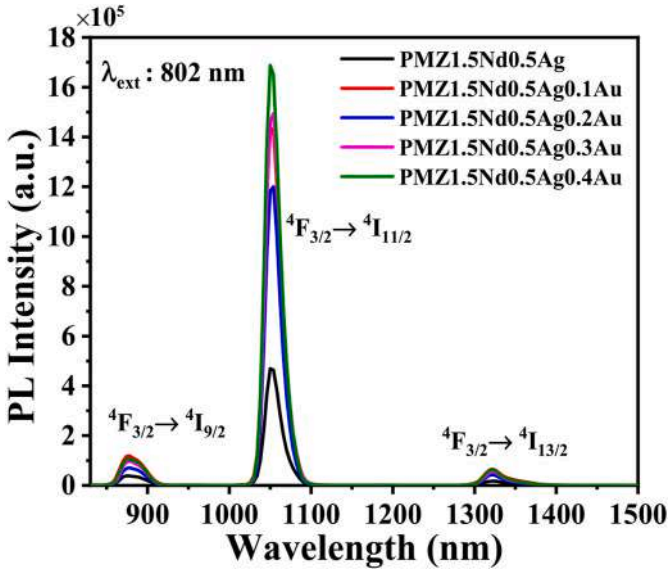

Fig. 13. PL of glass with different Au NPs contents.

area under the curve own by the glass embedded Au NPs with the one without Au NPs. Sample PMZ1.5Nd0.5Ag0·4Au show the utmost PL enhancement factor for a band around 1054 nm (3.49 times), meanwhile, sample PMZ1.5Nd0.5Ag0·2Au show the highest PL enhancement factor of 3.38 and 2.96 times for PL band around 878 nm and 1322 nm. The result revealed that tailoring NPs size could influence the local field surrounded Nd^{3+} ion and its PL behaviour [75]. The increase of Au NPs concentration would enlarge the average NPs size and modify the SPR strength [45]. Typically, wide separation of NPs allowed Ag and Au NPs to oscillate through their original plasmon frequency. Their weak Coulomb field would shift the SPR band away from one another [97]. However, narrowing the gap between NPs raises the Coulomb interaction and folded the plasmon field. Consequently, the natural plasmon field induced by Ag and Au NPs would be overlapped and create a new hybrid plasmon band [72]. The plasmon field may cause electron scattering or pure dephasing of the plasmon resonance [21]. The damping promotes a non-radiative path, thus altering the phonon-photon density of Nd^{3+} ion. This circumstance may cause a variation multiphoton relaxation rate at the different glass. The cross-relaxation within the transition state (where the excited REIs ion at higher state depopulated to less excited state) would result in a high non-radiative route at different transition states [29]. Thus, it is expected the transition $^4F_{3/2} \rightarrow {}^4I_{11/2}$ in sample PMZ1.5Nd0.5Ag0·2Au underwent PL quenching.

The result affirmed possible PL improvement with Au NPs inclusion which could materialize two ways. Firstly, the SPR induce a strong local field that raises the density of REIs that are responsible for PL. Secondly, it can be done through energy transfer from metal NPs to REIs nearby. It was argued that energy transfer (ET) could contribute to PL improvement. This is due to the large energy gap between the SPR band (463 nm and 503 nm) and the PL excitation (802 nm) [42] and also the short plasmon oscillation life-span ($\approx 10^{-14}$ s) of Ag and Au NPs compared to Nd^{3+} ($\approx 10^{-6}$ to 10^{-3} s) [3]. Thus, major PL improvement is credited to effective local field effect in proximity REIs. Conversely, PL quenching could be associated with predominant ET from Nd^{3+} ion to Au and Ag NPs (reabsorption by NPs), where the dipole-dipole interaction between the Nd^{3+} ion and the NPS become strong [12].

The radiative parameter such as electric line strength (S_{ed}), electric spontaneous transition probability (A_{ed}), magnetic spontaneous transition probability (A_{md}), radiative transition probability (A_{rad}), branching ratio (β_R), a radiative lifetime (τ_{rad}) of prepared glass is enlisted in Table 8. The bandwidth ($\Delta\lambda_{eff}$), stimulate cross-section emission (σ_P^E), bandwidth gain $\sigma_P^E \times \Delta\lambda_{eff}$ is disclosed in Table 9. The glass containing 0.2 mol% of Au NPs exhibit the highest branching ratio (0.45) for transition $^4F_{3/2} \rightarrow {}^4I_{11/2}$ which indicates a high possibility of attaining

Table 8
Radiative properties of the studied glasses.

Sample	Transition	λ(nm)	$S_{ed}(10 \times {}^{-20})$	$A_{ed}(s^{-1})$	$A_{md}(s^{-1})$	$A_{rad}(s^{-1})$	β_R	τ_{rad}(ms)
PMZ1.5Nd0.5 Ag	$^4F_{3/2} \rightarrow {}^4I_{13/2}$	1322	1.4377	368.38	0	368.38	0.0694	2.5795
	$^4F_{3/2} \rightarrow {}^4I_{11/2}$	1050	4.4226	2297.32	0	2297.32	0.4325	0.3724
	$^4F_{3/2} \rightarrow {}^4I_{9/2}$	874	2.9475	2626.351	0	2626.351	0.4945	0.1883
PMZ1.5Nd0.5Ag0·1Au	$^4F_{3/2} \rightarrow {}^4I_{13/2}$	1322	1.5414	394.949	0	394.949	0.072	2.406
	$^4F_{3/2} \rightarrow {}^4I_{11/2}$	1054	4.6347	2407.517	0	2407.517	0.4389	0.3542
	$^4F_{3/2} \rightarrow {}^4I_{9/2}$	878	2.9878	2662.244	0	2662.244	0.4853	0.1823
PMZ1.5Nd0.5Ag0·2Au	$^4F_{3/2} \rightarrow {}^4I_{13/2}$	1322	1.4616	374.509	0	374.509	0.0781	2.5373
	$^4F_{3/2} \rightarrow {}^4I_{11/2}$	1050	4.1876	2175.265	0	2175.265	0.4536	0.3892
	$^4F_{3/2} \rightarrow {}^4I_{9/2}$	878	2.4989	2226.622	0	2226.622	0.4643	0.2085
PMZ1.5Nd0.5Ag0·3Au	$^4F_{3/2} \rightarrow {}^4I_{13/2}$	1322	1.5087	386.588	0	386.588	0.0738	2.458
	$^4F_{3/2} \rightarrow {}^4I_{11/2}$	1054	4.4694	2321.646	0	2321.646	0.4432	0.3665
	$^4F_{3/2} \rightarrow {}^4I_{9/2}$	878	2.8162	2509.314	0	2509.314	0.4791	0.1909
PMZ1.5Nd0.5Ag0·4Au	$^4F_{3/2} \rightarrow {}^4I_{13/2}$	1322	1.4862	380.81	0	380.81	0.0735	2.4953
	$^4F_{3/2} \rightarrow {}^4I_{11/2}$	1050	4.4148	2293.269	0	2293.269	0.4424	0.3712
	$^4F_{3/2} \rightarrow {}^4I_{9/2}$	878	2.7937	2489.309	0	2489.309	0.4803	0.1929

Table 9
Estimated values of λ_p (in nm), $\Delta\lambda_{eff}$ (in nm), σ_P^E ($\times 10^{-24}$ cm^2), $\sigma_P^E \times \Delta\lambda_{eff}$ ($\times 10^{-23}$ cm^3) and the enhancement factor for the prepared glass.

Sample	λ_p		$\Delta\lambda_{eff}$	σ_P^E	$\sigma_P^E \times \Delta\lambda_{eff}$	Enhancement Factor
PMZ1.5Nd0.5 Ag	$^4F_{3/2} \rightarrow {}^4I_{13/2}$	1322	33.67	1.918	6.458	1.00
	$^4F_{3/2} \rightarrow {}^4I_{11/2}$	1050	22.12	7.246	16.028	1.00
	$^4F_{3/2} \rightarrow {}^4I_{9/2}$	874	35.34	2.489	8.796	1.00
PMZ1.5Nd0.5Ag0·1Au	$^4F_{3/2} \rightarrow {}^4I_{13/2}$	1322	26.34	2.629	6.924	2.04
	$^4F_{3/2} \rightarrow {}^4I_{11/2}$	1054	22.12	7.711	17.050	2.49
	$^4F_{3/2} \rightarrow {}^4I_{9/2}$	878	32.44	2.799	9.081	1.71
PMZ1.5Nd0.5Ag0·2Au	$^4F_{3/2} \rightarrow {}^4I_{13/2}$	1322	28.09	2.337	6.566	3.38
	$^4F_{3/2} \rightarrow {}^4I_{11/2}$	1050	23.23	6.534	15.176	3.13
	$^4F_{3/2} \rightarrow {}^4I_{9/2}$	878	33.67	2.256	7.595	2.96
PMZ1.5Nd0.5 Ag 0.3Au	$^4F_{3/2} \rightarrow {}^4I_{13/2}$	1322	26.28	2.579	6.778	2.62
	$^4F_{3/2} \rightarrow {}^4I_{11/2}$	1054	22.94	7.168	16.446	3.20
	$^4F_{3/2} \rightarrow {}^4I_{9/2}$	878	32.51	2.633	8.559	2.35
PMZ1.5Nd0.5 Ag 0.4Au	$^4F_{3/2} \rightarrow {}^4I_{13/2}$	1322	25.57	2.611	6.676	3.00
	$^4F_{3/2} \rightarrow {}^4I_{11/2}$	1050	22.16	7.220	16.000	3.50
	$^4F_{3/2} \rightarrow {}^4I_{9/2}$	878	33.14	2.562	8.491	2.60

that particular transition [33]. However, samples inserted with 0.1 mol % of Au NPs show the highest radiative transition probability A_{rad} for all transitions ($^4F_{3/2} \rightarrow {}^4I_{9/2}$, $^4F_{3/2} \rightarrow {}^4I_{11/2}$ and $^4F_{3/2} \rightarrow {}^4I_{13/2}$). It also revealed the maximum bandwidth gain ($\sigma_P^E \times \Delta\lambda_{eff}$) in the mentioned transition with the value of 6.92, 17.05 and 9.10 ($\times 10^{-23}$ cm^3) respectively. The gain-bandwidth parameter was used to determine the performance of glass as laser amplifiers. The high gain-bandwidth indicates its capability as a laser host for broadband amplifier applications [25]. Although the glass embedded with 0.4 mol% of Au NPs show the highest calculated stimulated cross-section emission for transitions ($^4F_{3/2} \rightarrow {}^4I_{11/2}$ and $^4F_{3/2} \rightarrow {}^4I_{13/2}$), however, the perturbation from non-radiative relaxation need to take into account. Thus, relying upon σ_P^E parameters or PL enhancement would be less practical in deciding the capability of the glass as an amplifier [98]. The measurement of PL decay may benefit in understanding the non-radiative trends in Nd^{3+} ion [73].

Fig. 14 is a partially schematic Nd^{3+} diagram that may provide a better vision of the PL mechanism through Ag and Au NPs inclusion. Firstly, the Nd^{3+} ions rapidly excite from ground state $^4I_{9/2}$ to the higher energy state at the excitation of 802 nm. Then, the exciting Nd^{3+} ions that reside at a higher energy state are spontaneously de-excited to the lower energy state through non-radiative relaxation. The Nd^{3+} ion that reached metastable state at $^4F_{5/2}$ usually had a longer lifetime compared to other transition states. A high population inversion in the metastable state would allow three lasing transitions; $^4F_{3/2} \rightarrow {}^4I_{13/2}$, $^4I_{11/2}$ and $^4I_{9/2}$.

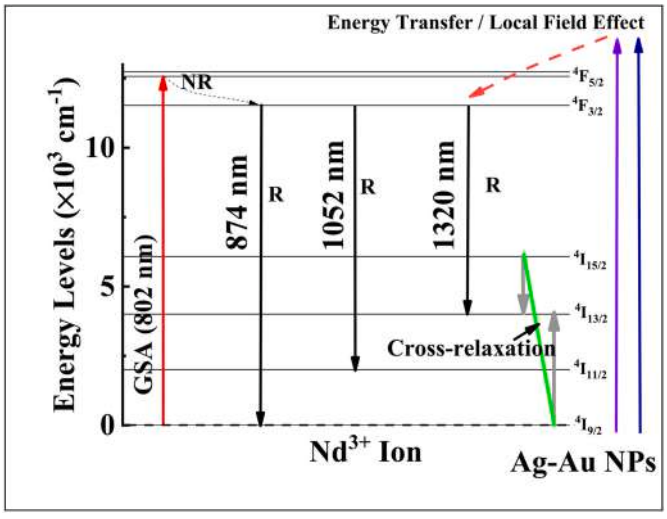

Fig. 14. Schematic partial energy diagram Nd^{3+} ion with presence Ag NP and Au NPs.

The Ag and Au NPs would assist PL through either local field effect and energy transfer that raised the number of excited electrons at the metastable state. Thus, the lifetime of the population depends on the NPs concentration incorporated into the glass which later interferes with the photon density of Nd^{3+} ion [44]. The cross-relaxation is possible in levels $^4F_{3/2} \rightarrow {}^4I_{15/2}$ and $^4I_{9/2} \rightarrow {}^4I_{15/2}$ [62]. Thus, coupling two metal NPs into the glass could be a new method to manipulate the PL of Nd^{3+} ion which can be useful in designing attractive optical material for medical or telecommunication use [70].

3.10. NIR PL spectra decay

Fig. 15 shows the decay lifetime of the prepared samples for transition $^4F_{3/2} \rightarrow {}^4I_{11/2}$. The curve was fitted using a bi-exponential function, involving slow and fast relaxation. The slow decay is dominant by $^4F_{3/2} \rightarrow {}^4I_{11/2}$ transition meanwhile fast decay is assigned to effective electron-phonon interaction through cross-relaxation process: $^4F_{3/2} \rightarrow {}^4I_{9/2}$ and $^4I_{15/2} + {}^4I_{15/2}$, as illustrated in Fig. 14 [99]. The previous reports mentioned that ET, multi-phonon relaxation, cross-relaxation could be the main contributor to the non-radiative (NR) mechanism which is dependent on the interparticle distance between identities [100,101]. The radiative lifetime (τ_{rad}), experimental lifetime (τ_{exp}), the ET efficiency (E_{ET}), non-radiative rate (W_{NR}) and quantum efficiency (η) are tabulated in Table 10 [102]. All glass demonstrates discrepancies

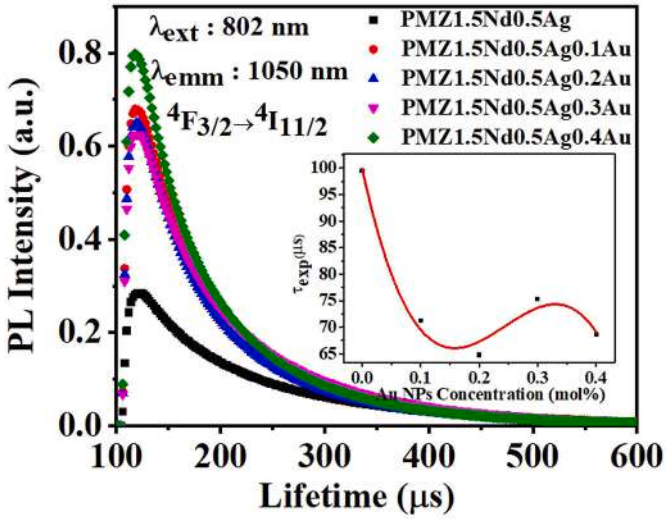

Fig. 15. NIR PL decay profile at the transition of $^4F_{3/2} \rightarrow {}^4I_{11/2}$ for all selected glass (Insert: The τ_{exp} in the function of Au NPs contents (mol%) inside the glass).

between τ_{rad} and τ_{exp} values which signify the existence of NR channels. Initially, the addition of Au NPs (0.1–0.2 mol%) into the glass shortens the τ_{exp} values. However as 0.3 mol% of Au NPs incorporated into the glass, the τ_{exp} values extended before it reduces slightly when inserted with 0.4 mol% of Au NPs. The variation of τ_{exp} at different Au NPs contents could be correlated with the Ag/Au NPs size proximity Nd^{3+} ion, lattice distortions/host defects and change in refractive index [103]. Despite having highest τ_{rad} (389.2 μs) values, sample PMZ1.5Nd0.5Ag0·2Au depicts the lowest τ_{exp} (64.79 μs) and η (16.65%). It also revealed a high rate of NR (0.0128μs^{-1}) and E_{ET} (0.349). According to Förster-Dexter theory, the efficiency of ET is proportional to the inverse of the sixth power of the distance between the ions [94]. Thus, high E_{ET} disclosed by PMZ1.5Nd0.5Ag0·2Au is probably due to the narrow distance between Nd^{3+} ions or Ag and Au NPs within the network, which reasonably lead to more NR path and low η values. However, deduces a small gap between ion-NPs as a basis of PL quenching could be debated since sample PMZ1.5Nd0.5Ag0·4Au contains high Au NPs contents than PMZ1.5Nd0.5Ag0.2Au. Thus, other than the inter-distance, the efficiency of Ag and Au NPs coupling needs to be considered as the cause of high W_{NR} and E_{ET}. The perturbation wave functions from the hybridization state (from the electronic state coupling) stimulate nonlinear effect [104]. This occurrence cause few spectroscopic responses in PL dynamics of Nd^{3+} ions, the radiation decay rate and scattering of the metal NPs [104]. The high electron scattering effect through NPs surface would cause high W_{NR} and influence the η parameter [105]. Essentially, the electron-electron scattering, electron-photon scattering, radiation and electron scattering by the NPs surface are the damping factor of SPR [106]. Besides, whenever the Ag and Au NPs surrounded by a medium like glass, additional surface scattering known as chemical interface damping (CID) affects the effective local field generated by SPR [106]. Thus, though PMZ1.5Nd0.5Ag0·2Au exhibit considerable high τ_{rad} and PL enhancement, due to damping, the rate of NR is sensibly high and lead to low η value. In the view of high damping effect from Ag and Au NPs, PMZ1.5Nd0.5Ag0.1 was contemplated as the good candidate for NIR laser host operated at 1.06 μm, considering its highest $\sigma_P^E \times \Delta\lambda_{eff}$ values and moderate η value among glass series.

4. Conclusion

This is the first time Nd^{3+}-doped zinc-sulfate-magnesium-phosphate glass were integrated with Ag and Au NPs via the melt-quenching method. The existence of Ag and Au NPs in the glass matrix was observed in the HRTEM micrograph with their mean size ranged from 4.47 to 7.03 nm. The SPR bands of Ag and Au NPs were detected at 463 and 503 nm, respectively. The SPR bands of Ag and Au NPs move towards each other when the NPs inter-spacing became narrow. The insertion of Au NPs enhanced the glass absorbance and PL intensity slightly. Thirteen optical absorption bands were evidenced in the range of 326–875 nm. The NIR PL bands were probed at 878 nm, 1054 nm and 1322 nm that were due to $^4F_{3/2} \rightarrow {}^4I_{9/2}$, $^4F_{3/2} \rightarrow {}^4I_{11/2}$ and $^4F_{3/2} \rightarrow {}^4I_{13/2}$ transitions, respectively. However, no significant PL improvement was evidenced from Ag–Au NPs plasmonic coupling due to the damping effects. The short NPs separation was argued to promote the non-radiative channel and led to PL intensity quenching. The optimum bandwidth gain parameters of 6.92, 17.05 and 9.10 ($\times 10^{-23}$ cm^3) were achieved for the PMZ1.5Nd0.5Ag0·1Au glass corresponding to the $^4F_{3/2} \rightarrow {}^4I_{9/2}$, $^4F_{3/2} \rightarrow {}^4I_{11/2}$ and $^4F_{3/2} \rightarrow {}^4I_{13/2}$ transitions, respectively. It indicated the potential of these samples as a laser amplifier functioning at 1.06 μm. The result demonstrated the potential of the proposed glass for the solid−state laser applications.

Credit author statement

N. N. Yusof: Conceptualization, Methodology, Software, Formal analysis, Investigation, Resources, Data curation, Validation, Writing – original draft, Visualization **S.Hashim**: Validation, Supervision, Project administration, Funding acquisition **S. K. Ghoshal**: Conceptualization, Methodology, Writing – review & editing, Supervision, Project administration, Funding acquisition **M.N Azlan**: Writing – review & editing, Funding acquisition **M.H.M. Zaid**: Validation, Writing – review & editing **Imed Boukhris**: Funding acquisition **Imen Kebaili**: Funding acquisition

Table 10
The radiative lifetime (τ_{rad}), experimental lifetime (τ_{exp}), the ET efficiency (E_{ET}), non-radiative rate (W_{NR}) and quantum efficiency (η) of the prepared glasses.

Glass code	τ_{rad} (μs)	τ_{exp} (μs)	W_{NR} (μs^{-1})	E_{ET}	η (%)
PMZ1.5Nd0.5 Ag	372.4	99.5	0.0074	–	26.71
PMZ1.5Nd0.5Ag0·1Au	354.2	71.2	0.0112	0.284	20.10
PMZ1.5Nd0.5Ag0·2Au	389.2	64.8	0.0129	0.349	16.65
PMZ1.5Nd0.5Ag0·3Au	366.5	75.3	0.0106	0.243	20.55
PMZ1.5Nd0.5Ag0·4Au	371.2	68.7	0.0119	0.309	18.51

Author statement

The manuscript entitled **'Spectrographic Analysis of Zinc-Sulfate-Magnesium-Phosphate Glass Containing Neodymium Ions: Impact of Silver–Gold Nanoparticles Plasmonic Coupling'** is original research work and has not been submitted/published in any journal. All authors have seen and approved the manuscript and have contributed significantly to the paper.

Ethical procedure

- The research meets all applicable standards with regard to the ethics of experimentation and research integrity, and the following is being certified/declared true.
- According to our experience and as along as authors and co-authors for several articles of concerned field, the paper has been submitted with full responsibility, following due ethical procedure, and there is no duplicate publication, fraud, plagiarism, or concerns about animal or human experimentation.

A disclosure/conflict of interest statement

- None of the authors of this paper has a financial or personal relationship with other people or organizations that could inappropriately influence or bias the content of the paper.
- It is to specifically state that "No Competing interests are at stake and there is No Conflict of Interest" with other people or organizations that could inappropriately influence or bias the content of the paper.

Declaration of competing interest

The authors declare that they have no known competing financial interests or personal relationships that could have appeared to influence the work reported in this paper.

Acknowledgement

The authors extend their appreciation to the Deanship of Scientific Research at King Khalid University, Saudi Arabia for funding this work through the Research Groups Program under grant number R.G.P.1/216/42. The authors gratefully acknowledge the financial support from UTM and the Malaysian Ministry of Education through Q. J130000.21A2.05E65 and Q. J130000.2554.20H65.

References

[1] A. Jagannathan, J. Gangareddy, R. Rajaramakrishna, K.M. Rajashekara, S.V. Rao, J. Kaewkhao, S. Kothan, A. El-Denglawey, Precursor based tuning of the nonlinear optical properties of Au-Ag bimetallic nanoparticles doped in oxy-fluoroborate glasses, J. Non-Cryst. Solids 561 (2021) 120766, https://doi.org/10.1016/J.Jnoncrysol.2021.120766.

[2] X.F. Zhang, Z.G. Liu, W. Shen, S. Gurunathan, Silver nanoparticles: synthesis, characterization, properties, applications, and therapeutic approaches, Int. J. Mol. Sci. 17 (2016) 1534, https://doi.org/10.3390/Ijms17091534.

[3] N.N. Yusof, S.K. Ghoshal, S.A. Jupri, M.N. Azlan, Synergistic effects of Nd^{3+} and Ag nanoparticles doping on spectroscopic attributes of phosphate glass, Opt. Mater. 110 (2020) 110403, https://doi.org/10.1016/J.Optmat.2020.110403.

[4] Y. Wei, H. Ebendorff-Heidepriem, J. Zhao, Recent advances in hybrid optical materials: integrating nanoparticles within A glass matrix, Adv. Opt. Mater. 7 (2019) 1–34, https://doi.org/10.1002/Adom.201900702.

[5] J. Haug, M. Dubiel, H. Kruth, H. Hofmeister, Structural characterization of bimetallic Ag-Au nanoparticles in glass, J. Phys. Conf. 190 (2009) 1–4, https://doi.org/10.1088/1742-6596/190/1/012124.

[6] S. Adichtchev, S. Sirotkin, G. Bachelier, L. Saviot, S. Etienne, B. Stephanidis, E. Duval, A. Mermet, High-order vibration modes of bimetallic Ag-Au nanoparticles embedded in glass, Phys. Rev. B Condens. Matter 79 (2009) 1–4, https://doi.org/10.1103/Physrevb.79.201402.

[7] M. Eichelbaum, K. Rademann, A. Hoell, D.M. Tatchev, W. Weigel, R. Stößer, G. Pacchioni, Photoluminescence of atomic gold and silver particles in soda-lime silicate glasses, Nanotechnology 19 (2008), https://doi.org/10.1088/0957-4484/19/13/135701.

[8] M. Epifani, C. Giannini, L. Tapfer, L. Vasanelli, Sol−Gel synthesis and characterization of Ag and Au nanoparticles in SiO_2, TiO_2, and ZrO_2 thin films, J. Am. Ceram. Soc. 83 (2000) 2385–2393.

[9] H. Gholamali, A. Shafiekhani, E. Darabi, S.M. Elahi, Synthesis of Ag and Au nanoparticles embedded in carbon film: optical, crystalline and topography analysis, Results Phys. 8 (2018) 336–340, https://doi.org/10.1016/J.Rinp.2017.12.033.

[10] J. Haug, H. Kruth, M. Dubiel, H. Hofmeister, S. Haas, D. Tatchev, A. Hoell, Asaxs study on the formation of core–shell Ag/Au nanoparticles in glass, Nanotechnology 20 (2009) 505705, https://doi.org/10.1088/0957-4484/20/50/505705.

[11] S.J. Lee, S. Kumar, J.W. Choi, V.Y. Kim, J.S. Lee, Copolymer particles with incorporated gold and silver nanoparticles to absorb short-wavelength scattering in full-color photonic glasses, Part. Part. Syst. Char. 36 (2019) 1–11, https://doi.org/10.1002/Ppsc.201900167.

[12] S.Q. Mawlud, A comparative enhancement of Au and Ag nps role on radiative properties in Sm^{3+} doped zinc-sodium tellurite glass: judd-ofelt parameter, Spectrochim. Acta Mol. Biomol. Spectrosc. 209 (2019) 78–84, https://doi.org/10.1016/J.Saa.2018.10.032.

[13] X. Meng, T. Shibayama, R. Yu, S. Takayanagi, S. Watanabe, Ion irradiation synthesis of Ag-Au bimetallic nanospheroids in sio 2 glass substrate with tunable surface plasmon resonance frequency, J. Appl. Phys. 114 (2013), https://doi.org/10.1063/1.4817725.

[14] S. Pramanik, S. Chattopadhyay, J.K. Das, U. Manju, G. De, Extremely fast Au-Ag alloy-dealloy associated reversible plasmonic modifications in SiO_2 films, J. Mater. Chem. C 4 (2016) 3571–3580, https://doi.org/10.1039/C5tc03123k.

[15] T. Som, B. Karmakar, Core-shell Au-Ag nanoparticles in dielectric nanocomposites with plasmon-enhanced fluorescence: a new paradigm in antimony glasses, Nano Res. 2 (2009) 607–616, https://doi.org/10.1007/S12274-009-9061-4.

[16] H. Tao, T. Hu, J. Yan, J. Di, A comparative study of different reagentless plasmon sensors based on Ag-Au alloy nanoparticles for detection of Hg, Sensor. Actuator. B Chem. 208 (2015) 43–49, https://doi.org/10.1016/J.Snb.2014.11.003.

[17] I.M. Danmallam, S.K. Ghoshal, R. Ariffin, I. Bulus, Europium luminescence in silver and gold nanoparticles Co-embedded phosphate glasses: judd-ofelt calculation, Opt. Mater. 105 (2020) 109889, https://doi.org/10.1016/J.Optmat.2020.109889.

[18] C. Calahoo, L. Wondraczek, Ionic glasses: structure, properties and classification, J. Non-Cryst. Solids X 8 (2020), https://doi.org/10.1016/J.Nocx.2020.100054.

[19] W.C. Wang, Q.H. Le, Q.Y. Zhang, L. Wondraczek, Fluoride-sulfophosphate glasses as hosts for broadband optical amplification through transition metal activators, J. Mater. Chem. C (2017) 7969–7976, https://doi.org/10.1039/C7tc01853c.

[20] N.N. Yusof, S.K. Ghoshal, S.A. Jupri, Luminescence of neodymium ion-activated magnesium zinc sulfophosphate glass: role of titanium nanoparticles sensitization, Opt. Mater. 109 (2020) 110390, https://doi.org/10.1016/J.Optmat.2020.110390.

[21] N.N. Yusof, S.K. Ghoshal, S.A. Jupri, Spectroscopic properties of neodymium doped magnesium zinc sulfophosphate glass: synergistic effects of titanium and silver nanoparticles embedment, Opt. Mater. 109 (2020) 110266, https://doi.org/10.1016/J.Optmat.2020.110266.

[22] M. Eichelbaum, K. Rademann, Plasmonic enhancement or energy transfer on the luminescence of gold-, silver-, and lanthanide-doped silicate glasses and its potential for light-emitting devices, Adv. Funct. Mater. 19 (2009) 2045–2052, https://doi.org/10.1002/Adfm.200801892.

[23] J. Shin, K. Jang, K.S. Lim, I.B. Sohn, Y.C. Noh, J. Lee, Formation and control of Au and Ag nanoparticles inside borate glasses using femtosecond laser and heat treatment, Appl. Phys. Mater. Sci. Process 93 (2008) 923–927, https://doi.org/10.1007/S00339-008-4759-9.

[24] V.A.G. Rivera, Y. Ledemi, S.P.A. Osorio, D. Manzani, Y. Messaddeq, L.A.O. Nunes, E. Marega, Efficient plasmonic coupling between Er^{3+}:(Ag/Au) in tellurite glasses, J. Non-Cryst. Solids 358 (2012) 399–405, https://doi.org/10.1016/J.Jnoncrysol.2011.10.008.

[25] K. Siva Rama Krishna Reddy, K. Swapna, S. Mahamuda, M. Venkateswarulu, A. S. Rao, Structural, optical and photoluminescence properties of alkaline-earth boro tellurite glasses doped with trivalent neodymium for 1.06 Mm optoelectronic devices, Opt. Mater. 111 (2021) 110615, https://doi.org/10.1016/J.Optmat.2020.110615.

[26] P. Aryal, H.J. Kim, A. Khan, S. Saha, S.J. Kang, S. Kothan, Y. Yamsuk, J. Kaewkhao, Development of Eu^{3+}-doped phosphate glass for red luminescent solid-state optical devices, J. Lumin. 227 (2020) 117564, https://doi.org/10.1016/J.Jlumin.2020.117564.

[27] B. Karmakar, Functional Glasses And Glass-Ceramics: Processing, Properties And Applications, 2017, https://doi.org/10.1016/C2015-0-04249-6.

[28] Q.H. Le, T. Palenta, O. Benzine, K. Griebenow, R. Limbach, E.I. Kamitsos, L. Wondraczek, Formation, structure and properties of fluoro-sulfo-phosphate poly-anionic glasses, J. Non-Cryst. Solids 477 (2017) 58–72, https://doi.org/10.1016/J.Jnoncrysol.2017.09.043.

[29] S.A. Jupri, S.K. Ghoshal, N.N. Yusof, M.F. Omar, K. Hamzah, G. Krishnan, Influence of surface plasmon resonance of Ag nanoparticles on photoluminescence of Ho^{3+} ions in magnesium-zinc-sulfophosphate glass system, Opt Laser. Technol. 126 (2020) 106134, https://doi.org/10.1016/J.Optlastec.2020.106134.

[30] F. Ahmadi, Z. Ebrahimpour, A. Asgari, Titania nanoparticles embedded Er^{3+}-Sm^{3+} Co-doped sulfophosphate glass: judd-ofelt parameters and spectroscopic properties enhancement, J. Alloys Compd. 843 (2020) 155982, https://doi.org/10.1016/J.Jallcom.2020.155982.

[31] N.N. Yusof, S.K. Ghoshal, S.A. Jupri, M.N. Azlan, Nd^{3+} doped magnesium zinc sulfophosphate glass: new candidate for up-conversion solid state laser host, Opt. Mater. 109 (2020) 110299, https://doi.org/10.1016/J.Optmat.2020.110299.

[32] N.N. Yusof, S.K. Ghoshal, R. Arifin, A. Awang, H.S. Tewari, K. Hamzah, Self-cleaning and spectral attributes of erbium doped sodium-zinc-tellurite glass: role of titania nanoparticles, J. Non-Cryst. Solids (2017) 1–14, https://doi.org/10.1016/J.Jnoncrysol.2017.10.044.

[33] F. Ahmadi, R. Hussin, S.K. Ghoshal, On the optical properties of Er^{3+} ions activated magnesium zinc sulfophosphate glass: role of silver nanoparticles sensitization, J. Lumin. 204 (2018) 95–103, https://doi.org/10.1016/J.Memsci.2015.12.065.

[34] D.D. Ramteke, R.E. Kroon, H.C. Swart, Infrared emission spectroscopy and upconversion of zno-Li2o-Na2o-P2o5 glasses doped with Nd^{3+} ions, J. Non-Cryst. Solids 457 (2017) 157–163, https://doi.org/10.1016/J.Jnoncrysol.2016.12.006.

[35] I.I. Pm, W.T. Carnall, P.R. Fields, K. Rajnak, Spectral intensities of the trivalent lanthanides and actinides in solution. Ii. Pm^{3+}, Sm^{3+}, Eu^{3+}, Gd^{3+}, Tb^{3+}, Dy^{3+}, and Ho^{3+}, J. Chem. Phys. (1968) 4412, https://doi.org/10.1063/1.1669892.

[36] Y.A. Tanko, S.K. Ghoshal, M.R. Sahar, Ligand field and judd-ofelt intensity parameters of samarium doped tellurite glass, J. Mol. Struct. 1117 (2016) 64–68, https://doi.org/10.1016/J.Molstruc.2016.03.083.

[37] F. Gao, S. Zhang, Investigation of mechanism of nephelauxetic effect, J. Phys. Chem. Solid. 58 (1997) 1991–1994, https://doi.org/10.1016/S0022-3697(96)00139-4.

[38] N.M. Yusoff, M.R. Sahar, The incorporation of silver nanoparticles in samarium doped magnesium tellurite glass: effect on the characteristic of bonding and local structure, Phys. B Condens. Matter (2015) 470–471, https://doi.org/10.1016/J.Physb.2015.04.029, 6–14.

[39] W. Seeber, D. Ehrt, H. Ebendorff-Heidepriem, Spectroscopic and laser properties of $Ce^{3+}Cr^{3+}Nd^{3+}$ Co-doped fluoride phosphate and phosphate glasses, J. Non-Cryst. Solids 171 (1994) 94–104, https://doi.org/10.1016/0022-3093(94)90036-1.

[40] S.V.J. Lakshman, S. Buddhudu, Racah and judd-ofelt parameters for Pr^{3+}, Nd^{3+}, and Er^{3+} ions in A laser liquid, J Quant Spectrosc Radiat Transf 24 (1980) 251–257, https://doi.org/10.1016/0022-4073(80)90067-9.

[41] J. Zhao, Z. Yang, C. Yu, J. Qiu, Z. Song, Influence of glass composition on photoluminescence from Ge^{2+} or Ag nano-cluster in germanate glasses for white light-emitting diodes, J. Am. Ceram. Soc. 102 (2019) 1169–1179, https://doi.org/10.1111/Jace.16004.

[42] I. Abdullahi, S. Hashim, S.K. Ghoshal, L. Sa'adu, Modified structure and spectroscopic characteristics of Sm^{3+}/Dy^{3+} Co-activated barium-sulfur-telluro-borate glass host: role of plasmonic gold nanoparticles inclusion, Opt Laser. Technol. 132 (2020) 106486, https://doi.org/10.1016/J.Optlastec.2020.106486.

[43] T. Wei, Y. Tian, C. Tian, X. Jing, M. Cai, J. Zhang, L. Zhang, S. Xu, Comprehensive evaluation of the structural, absorption, energy transfer, luminescent properties and near-infrared applications of the neodymium doped germanate glass, J. Alloys Compd. 618 (2015) 95–101, https://doi.org/10.1016/J.Jallcom.2014.08.139.

[44] S.Q. Mawlud, Physical and thermal properties of gold nanoparticles embedded Nd^{3+}- doped borophosphate glasses: spectroscopic parameters, J. Lumin. 236 (2021) 118079, https://doi.org/10.1016/J.Jlumin.2021.118079.

[45] G. Jagannath, B. Eraiah, K. Jayanthi, S.R. Keshri, S. Som, G. Vinitha, A. G. Pramod, K.N. Krishnakanth, G. Devarajulu, S. Balaji, S. Venugopal Rao, K. Annapurna, S. Das, A.R. Allu, Influence of gold nanoparticles on the nonlinear optical and photoluminescence properties of Eu_2O_3 doped alkali borate glasses, Phys. Chem. Chem. Phys. 22 (2020) 2019–2032, https://doi.org/10.1039/C9cp05783h.

[46] A. Jagannathan, R. Rajaramakrishna, K.M. Rajashekara, J. Gangareddy, V. Pattar K, V.R. S, E. B, J. Angadi V, J. Kaewkhao, S. Kothan, Investigations on nonlinear

optical properties of gold nanoparticles doped fluoroborate glasses for optical limiting applications, J. Non-Cryst. Solids 538 (2020) 120010, https://doi.org/10.1016/J.Jnoncrysol.2020.120010.
[47] T.Y. Lim, H. Wagiran, R. Hussin, S. Hashim, M.A. Saeed, Physical and optical properties of dysprosium ion doped strontium borate glasses, Phys. B Condens. Matter 451 (2014) 63–67, https://doi.org/10.1016/J.Physb.2014.06.028.
[48] J.T. James, J.K. Jose, M. Manjunatha, K. Suresh, A. Madhu, Structural, luminescence and nmr studies on Nd^{3+}-doped sodium–calcium-borate glasses for lasing applications, Ceram. Int. 46 (2020) 27099–27109, https://doi.org/10.1016/J.Ceramint.2020.07.187.
[49] T. Som, B. Karmakar, Synthesis and enhanced photoluminescence in novel aucoreau-agshell nanoparticles embedded Nd^{3+}-doped antimony oxide glass hybrid nanocomposites, J Quant Spectrosc Radiat Transf 112 (2011) 2469–2479, https://doi.org/10.1016/J.Jqsrt.2011.06.015.
[50] N. Shasmal, B. Karmakar, Enhancement of photoluminescence in white light emitting glasses by localized surface plasmons of Ag and Au nanoparticles, Chem. Phys. Lett. 754 (2020) 137713, https://doi.org/10.1016/J.Cplett.2020.137713.
[51] P. Taylor, T. Som, B. Karmakar, Plasmonic Au X Ag Y bimetallic alloy nanoparticles enhanced photoluminescence upconversion of Er ions in antimony glass hybrid nanocomposites, J. Mod. Opt. 58 (2011) 37–41, https://doi.org/10.1080/09500340.2011.586472.
[52] G. Lofrano, G. Libralato, Nanotechnologies For Environmental Remediation, Springer, Switzerland, 2017, https://doi.org/10.1007/978-3-319-53162-5.
[53] M.H.U. Bhuiyan, R. Saidur, M.A. Amalina, R.M. Mostafizur, A.K.M.S. Islam, Effect of nanoparticles concentration and their sizes on surface tension of nanofluids, Procedia Eng. 105 (2015) 431–437, https://doi.org/10.1016/J.Proeng.2015.05.030.
[54] I. Soltani, S. Hraiech, K. Horchani-Naifer, H. Elhouichet, B. Gelloz, M. Férid, Growth of silver nanoparticles stimulate spectroscopic properties of Er^{3+} doped phosphate glasses: heat treatment effect, J. Alloys Compd. 686 (2016) 556–563, https://doi.org/10.1016/J.Jallcom.2016.06.027.
[55] A. Langar, N. Sdiri, H. Elhouichet, M. Ferid, Structure and electrical characterization of zno-Ag phosphate glasses, Results Phys. 7 (2017) 1022–1029, https://doi.org/10.1016/J.Rinp.2017.02.028.
[56] D. Möncke, S. Sirotkin, E. Stavrou, E.I. Kamitsos, L. Wondraczek, D. Möncke, S. Sirotkin, E. Stavrou, E.I. Kamitsos, Partitioning and structural role of Mn and Fe ions in ionic sulfophosphate glasses, J. Chem. Phys. 224509 (2014) 141, https://doi.org/10.1063/1.4903191.
[57] A.K. Yadav, P. Singha, A review of structure of oxide glasses by Raman spectroscopy, RSC Adv. (2015), https://doi.org/10.1039/C5ra13043c.
[58] M.V.R. Rao, Y. Gandhi, L.S. Rao, G. Sahayabaskaran, N. Veeraiah, Electrical and spectroscopic properties of Fe_2O_3 doped Na_2SO_4–BaO–P_2O_5 glass system, Mater. Chem. Phys. 126 (2011) 58–68, https://doi.org/10.1016/J.Matchemphys.2010.12.010.
[59] K. Linganna, R. Narro-García, P. Manasa, H. Desirena, E. De Rosa, C. K. Jayasankar, Effect of BaF_2 addition on luminescence properties of Er^{3+}/Yb^{3+} Co-doped phosphate glasses, J. Rare Earths 36 (2018) 58–63, https://doi.org/10.1016/J.Jre.2017.06.008.
[60] K.H. Sadok, M. Haouari, H. Ben Ouada, Effect of Na_2SO_4 substitution for Na_2O on the structural and electrical properties of A sodium borophosphate glass, J. Alloys Compd. 778 (2018) 878–888, https://doi.org/10.1016/J.Jallcom.2018.11.203.
[61] S.A. Jupri, S.K. Ghoshal, M.F. Omar, N.N. Yusof, Spectroscopic traits of holmium in magnesium zinc sulfophosphate glass host : judd-ofelt evaluation, J. Alloys Compd. 753 (2018) 446–456, https://doi.org/10.1016/J.Jallcom.2018.04.218.
[62] G. Neelima, K. Venkata Krishnaiah, N. Ravi, K. Suresh, K. Tyagarajan, T. Jayachandra Prasad, Investigation of optical and spectroscopic properties of neodymium doped oxyfluoro-titania-phosphate glasses for laser applications, Scripta Mater. 162 (2019) 246–250, https://doi.org/10.1016/J.Scriptamat.2018.11.018.
[63] K.S. Rao, V.R. Kumar, Y. Zhydachevskii, A. Suchocki, M. Piasecki, Y. Gandhi, V. R. Kumar, N. Veeraiah, Luminescence emission features of Nd^{3+} ions in PbO–Sb_2O_3 glasses mixed with $Sc_2O_3/Y_2O_3/HFO_2$, Opt. Mater. 69 (2017) 181–189, https://doi.org/10.1016/J.Optmat.2017.04.025.
[64] L. Chen, X. Deng, E. Zhao, X. Chen, S. Xue, W. Zhang, S. Chen, Z. Zhao, W. Zhang, T.S. Chan, The effect of electron cloud expansion on the red luminescence of $Sr_4Al_{14}O_{25}:Mn^{4+}$ revealed by calculation of the Racah parameters, J. Alloys Compd. 613 (2014) 312–316, https://doi.org/10.1016/J.Jallcom.2014.06.029.
[65] W.T. Carnall, Electronic energy levels in the trivalent lanthanide aquo ions. I. Pr^{3+}, Nd^{3+}, Pm^{3+}, Sm^{3+}, Dy^{3+}, Ho^{3+}, Er^{3+}, and Tm^{3+}, J. Chem. Phys. 49 (1968) 4424, https://doi.org/10.1063/1.1669893.
[66] S. Adachi, Spectroscopy of Cr^{3+} activator: tanabe−Sugano diagram and Racah parameter analysis, J. Lumin. 232 (2021) 117844, https://doi.org/10.1016/J.Jlumin.2020.117844.
[67] F. Ahmadi, R. Hussin, S.K.K. Ghoshal, Spectroscopic attributes of Sm^{3+} doped magnesium zinc sulfophosphate glass: effects of silver nanoparticles inclusion, Opt. Mater. J. 73 (2017) 268–276, https://doi.org/10.1016/J.Jallcom.2017.03.212.
[68] N.N. Yusof, S.K. Ghoshal, M.N. Azlan, Optical properties of titania nanoparticles embedded Er^{3+} -doped tellurite glass: judd-ofelt analysis, J. Alloys Compd. 724 (2017) 1083–1092, https://doi.org/10.1016/J.Jallcom.2017.07.102.
[69] G.Y. Shakhgildyan, M.Z. Ziyatdinova, M.P. Vetchinnikov, S.V. Lotarev, V. I. Savinkov, N.N. Presnyakova, E.V. Lopatina, G.A. Vilkovisky, V.N. Sigaev, Thermally-induced precipitation of gold nanoparticles in phosphate glass: effect on the optical properties of Er^{3+} ions, J. Non-Cryst. Solids 550 (2020) 120408, https://doi.org/10.1016/J.Jnoncrysol.2020.120408.
[70] G.Y. Shakhgil'dyan, M.Z. Ziyatdinova, V.V. Kovgar, S.V. Lotarev, V.N. Sigaev, I. V. Prusova, Effect of gold nanoparticles on the spectral luminescence properties of Eu^{3+}-doped phosphate glass, glass and ceramics (English translation of steklo I keramika) 76 (2019) 121–125, https://doi.org/10.1007/S10717-019-00147-W.
[71] A.A. Maradudin, J.R. Sambles, W.L. Barnes, Modern Plasmonics, Elsevier, Oxford, 2014, https://doi.org/10.1016/B978-0-444-59526-3.00016-1.
[72] A. Hazra, S.M. Hossain, A.K. Pramanick, M. Ray, Gold-silver nanostructures: plasmon-plasmon interaction, Vacuum 146 (2016) 437–443, https://doi.org/10.1016/J.Vacuum.2017.05.016.
[73] J.A. Scholl, A. García-Etxarri, A.L. Koh, J.A. Dionne, Observation of quantum tunneling between two plasmonic nanoparticles, Nano Lett. 13 (2013) 564–569, https://doi.org/10.1021/Nl304078v.
[74] H. Cha, D. Lee, J.H. Yoon, S. Yoon, Plasmon coupling between silver nanoparticles: transition from the classical to the quantum regime, J. Colloid Interface Sci. 464 (2016) 18–24, https://doi.org/10.1016/J.Jcis.2015.11.009.
[75] M.S.A. Mohd Saidi, S.K. Ghoshal, K. Hamzah, R. Arifin, M.F. Omar, M.K. Roslan, E.S. Sazali, Visible light emission from Dy^{3+}Doped tellurite glass: role of silver and titania nanoparticles Co-embedment, J. Non-Cryst. Solids 502 (2018) 198–209, https://doi.org/10.1016/J.Jnoncrysol.2018.09.012.
[76] S.Q. Mawlud, M.M. Ameen, M.R. Sahar, K.F. Ahmed, Plasmon-enhanced luminescence of samarium doped sodium tellurite glasses embedded with gold nanoparticles: judd-ofelt parameter, J. Lumin. 190 (2017) 468–475, https://doi.org/10.1016/J.Jlumin.2017.06.004.
[77] A.M. Garcia, S. Diego, L.R.P. Kassab, D.M. Silva, C.B. De Araújo, J.A.M. Garcia, D. S. Da Silva, C.B. De Araújo, A.M. Garcia, S. Diego, L.R.P. Kassab, D.M. Silva, C. B. De Araújo, Silver nanoparticles enhanced photoluminescence of Nd^{3+} doped germanate glasses at 1064 nm, Opt. Mater. 60 (2016) 25–29, https://doi.org/10.1016/J.Optmat.2016.07.006.
[78] Y. Ma, Z. Chen, Y. Chu, Y. Yang, Y. Liu, H. Li, J. Peng, N. Dai, J. Li, L. Yang, Regulation of gold nanoparticles for the rare earth luminescence enhancement based on nanoporous silica glass, J. Lumin. 204 (2018) 104–109, https://doi.org/10.1016/J.Jlumin.2018.07.041.
[79] C.S.S.R. Kumar, Uv-Vis And Photoluminescence Spectroscopy For Nanomaterials Characterization, Springer, New York, 2013, https://doi.org/10.1007/978-3-642-27594-4.
[80] P.K. Jain, X. Huang, I.H. El-Sayed, M.A. El-Sayed, Review of some interesting surface plasmon resonance-enhanced properties of noble metal nanoparticles and their applications to biosystems, Plasmonics 2 (2007) 107–118, https://doi.org/10.1007/S11468-007-9031-1.
[81] N. Shasmal, B. Karmakar, Localized surface plasmon absorption and photoluminescence of in situ-generated nano silver in A novel chloroborosilicate glass and glass ceramics, Plasmonics (2014), https://doi.org/10.1007/S11468-014-9793-1.
[82] C. Kittel, Introduction To Solid State Physics, Wiley, Berkeley, 2005.
[83] F. Ahmadi, R. Hussin, S.K. Ghoshal, Tailored optical properties of Dy^{3+} doped magnesium zinc sulfophosphate glass: function of silver nanoparticles embedment, J. Non-Cryst. Solids 499 (2018) 131–141, https://doi.org/10.1016/J.Optmat.2017.08.021.
[84] M. Saad, W. Stambouli, S.A. Mohamed, H. Elhouichet, Ag nanoparticles induced luminescence enhancement of Eu^{3+} doped phosphate glasses, J. Alloys Compd. 705 (2017) 550–558, https://doi.org/10.1016/J.Jallcom.2016.12.410.
[85] I. Soltani, S. Hraiech, K. Horchani-Naifer, J. Massera, L. Petit, M. Ferid, M. Férid, Thermal, structural and optical properties of Er^{3+} doped phosphate glasses containing silver nanoparticles, J. Non-Cryst. Solids 438 (2016) 67–73, https://doi.org/10.1016/J.Jnoncrysol.2015.12.022.
[86] D. Rajesh, R.J. Amjad, M. Reza Dousti, A.S.S. De Camargo, Enhanced vis and nir emissions of Pr^{3+} ions in tzyn glasses containing silver ions and nanoparticles, J. Alloys Compd. 695 (2017) 607–612, https://doi.org/10.1016/J.Jallcom.2016.11.058.
[87] A. Herrera, N.M. Balzaretti, Effect of gold nanoparticles in broadband near-infrared emission of Pr^{3+} doped B_2O_3–PbO–$Bi_2O{=}O_3$–GeO_2 glass, J. Lumin. 181 (2017) 147–152, https://doi.org/10.1016/J.Jlumin.2016.09.013.
[88] A.M. Hamza, M.K. Halimah, F.D. Muhammad, K.T. Chan, Physical properties, ligand field and judd-ofelt intensity parameters of bio-silicate borotellurite glass system doped with erbium oxide, J. Lumin. (2018), https://doi.org/10.1016/J.Jlumin.2018.11.038.
[89] Y.C. Ratnakaram, N.V. Srihari, A.V. Kumar, D.T. Naidu, R.P.S. Chakradhar, Optical absorption and photoluminescence properties of Nd^{3+}Doped mixed alkali phosphate glasses-spectroscopic investigations, Spectrochim. Acta Mol. Biomol. Spectrosc. 72 (2009) 171–177, https://doi.org/10.1016/J.Saa.2008.09.008.
[90] Y.B. Xiao, Y. Ji, J.L. Liu, W.C. Wang, Nd^{3+}-Doped mixed-anion fluoro-sulfo-phosphate glass for 1.06 μm solid-state laser, J. Non-Cryst. Solids (2019) 522, https://doi.org/10.1016/J.Jnoncrysol.2019.119586.
[91] S.Y. Moustafa, M.R. Sahar, S.K. Ghoshal, Spectroscopic attributes of Er^{3+} ions in antimony phosphate glass incorporated with Ag nanoparticles: judd-ofelt analysis, J. Alloys Compd. 712 (2017) 781–794, https://doi.org/10.1016/J.Jallcom.2017.04.106.
[92] M. Seshadri, V. De C. Dos Anjos, M.J.V. Bell, Luminescent Glass For Lasers And Solar Concentrators, Luminescence - An Outlook On The Phenomena And Their Applications, 2016, https://doi.org/10.5772/65057.
[93] Y. Cao, C. Shao, F. Wang, W. Xu, S. Wang, L. Hu, C. Yu, Local environment regulation and performance analysis in Nd^{3+}-doped SiO_2-$Al(PO_3)_3$ binary composite glass, J. Non-Cryst. Solids (2017), https://doi.org/10.1016/J.Jnoncrysol.2017.10.051, 0–1.

[94] M. Seshadri, V. Anjos, M.J.V. Bell, Energy transfer process and radiative properties of 1.06 μm emission in Nd^{3+}Doped TeO_2-ZnO-Na_2O glasses, J. Lumin. 196 (2018) 399–405, https://doi.org/10.1016/J.Jlumin.2017.12.055.
[95] K. Mariselvam, R.A. Kumar, P. Manasa, Spectroscopic investigations of neodymium doped barium bismuth fluoroborate glasses, Infrared Phys. Technol. 91 (2018) 18–26, https://doi.org/10.1016/J.Infrared.2018.03.021.
[96] J. Suresh Kumar, K. Pavani, S.R. Gavinho, M. Seshadri, V. Anjos, M.J.V. Bell, F. N. Freire, M.A. Valente, M.J. Soares, M.P.F. Graça, Temperature dependent upconversion and spectroscopic properties of Nd^{3+}Doped barium bismuth tellurite glasses, J. Non-Cryst. Solids 498 (2018) 89–94, https://doi.org/10.1016/J.Jnoncrysol.2018.05.031.
[97] P. Nordlander, C. Oubre, E. Prodan, K. Li, M.I. Stockman, Plasmon hybridization in nanoparticle dimers, Nano Lett. 4 (2004) 899–903, https://doi.org/10.1021/Nl049681c.
[98] H. Largot, K.E. Aiadi, M. Ferid, S. Hraiech, C. Bouzidi, C. Charnay, K. Horchani-Naifer, Spectroscopic investigations of Sm^{3+}Doped phosphate glasses: judd-ofelt analysis, Phys. B Condens. Matter 552 (2019) 184–189, https://doi.org/10.1016/J.Physb.2018.10.010.
[99] E. Kolobkova, A. Yasukevich, N. Kuleshov, N. Nikonorov, A. Babkina, Concentration dependence of spectroscopic properties and energy transfer analysis of the fluorophosphate glasses with small phosphates content doped with Nd^{3+} ions, J. Non-Cryst. Solids 526 (2019) 119703, https://doi.org/10.1016/J.Jnoncrysol.2019.119703.
[100] T.M. Machado, R.F. Falci, I.L. Silva, V. Anjos, M.J.V. Bell, M.A.P. Silva, Erbium 1.55μm luminescence enhancement due to copper nanoparticles plasmonic activity in tellurite glasses, Mater. Chem. Phys. 224 (2019) 73–78, https://doi.org/10.1016/J.Matchemphys.2018.11.059.
[101] H. Fares, I. Jlassi, S. Hraiech, H. Elhouichet, M. Férid, Radiative parameters of Nd^{3+}-doped titanium and tungsten modified tellurite glasses for 1.06μm laser materials, J Quant Spectrosc Radiat Transf 147 (2014) 224–232, https://doi.org/10.1016/J.Jqsrt.2014.05.029.
[102] P.R. Rani, M. Venkateswarlu, K. Swapna, S. Mahamuda, R.A. Talewar, C. B. Annapurna Devi, A.S. Rao, Nir photoluminescence studies of Nd^{3+}Doped B_2O_3–BaF_2–PbF_2–Al_2O_3 glasses for 1.063 μm laser applications, J. Lumin. 229 (2021), https://doi.org/10.1016/J.Jlumin.2020.117701.
[103] G.M. Cai, N. Yang, H.X. Liu, J.Y. Si, Y.Q. Zhang, Single-phased and color tunable $LiSrBO_3$:Dy^{3+}, Tm^{3+}, Eu^{3+} phosphors for white-light-emitting application, J. Lumin. 187 (2017) 211–220, https://doi.org/10.1016/J.Jlumin.2017.03.017.
[104] E. Cao, W. Lin, M. Sun, W. Liang, Y. Song, Exciton-plasmon coupling interactions: from principle to applications, Nanophotonics 7 (2018) 145–167, https://doi.org/10.1515/Nanoph-2017-0059.
[105] V.G. Kravets, A.V. Kabashin, W.L. Barnes, A.N. Grigorenko, Plasmonic surface lattice resonances: a review of properties and applications, Chem. Rev. 118 (2018) 5912–5951, https://doi.org/10.1021/Acs.Chemrev.8b00243.
[106] A. Kheirandish, N. Sepehri Javan, H. Mohammadzadeh, Modified drude model for small gold nanoparticles surface plasmon resonance based on the role of classical confinement, Sci. Rep. 10 (2020) 1–10, https://doi.org/10.1038/S41598-020-63066-9.